Title: Membrane cholesterol regulates TRPV4 function, cytoskeletal expression and the cellular response to tension

Authors: Monika Lakk[1], Grace F. Hoffmann[1] , Aruna Gorusupudi[1], Paul S. Bernstein[1], Trine Toft-Bertelsen[2], Nanna MacAulay[2] and David Križaj[1,3,4]

[1]Department of Ophthalmology & Visual Sciences, University of Utah School of Medicine, Salt Lake City, Utah 84132 USA; [2]Department of Neuroscience, University of Copenhagen, 2200 Copenhagen, Denmark; [3]Department of Bioengineering; [4]Department of Neurobiology & Anatomy, University of Utah, Salt Lake City, Utah 84132 USA

Correspondence to: David Križaj, 65 N Mario Capecchi Drive, Bldg. 523, Room S4140 JMEC, Salt Lake City, UT 84132. david.krizaj@hsc.utah.edu

Short Title: Cholesterol-TRPV4 interactions

Funding Sources: National Institutes of Health (R01EY027920, R01EY011600, P30EY014800), Glaucoma Research Foundation, ALSAM-Skaggs Foundation, The Neuroscience Initiative at the University of Utah and and Unrestricted Grant from Research to Prevent Blindness to Department of Ophthalmology at the University of Utah

Abbreviations: AA, arachidonic acid; αSMA, alpha smooth muscle actin; BSA, bovine serum albumin; $[Ca^{2+}]_i$, intracellular calcium concentration; C/P, cholesterol/phosphatidylcholine ratio; ECM, extracellular matrix; EET, epoxyeicosatrienoic acid; extracellular matrix; F-actin, filamentous actin; FBS, fetal bovine serum; HRP, horse-radish peroxidase; HTS, hypotonic stimulation; ir, immunoreactivity, IOP, intraocular pressure; MβCD, methyl-beta-cyclodextrin; POAG, primary open angle glaucoma; qRT-PCR, quantitative real-time polymerase chain reaction; RIPA, radioimmunoprecipitation assay; SACs, stretch activated channels; SMCs, smooth muscle cell; TM, trabecular meshwork; TRPV4, transient receptor potential vanilloid isoform 4;

Abstract

Cholesterol plays important roles in the regulation of membrane viscoelasticity, protein function and cellular health but despite its association with debilitating pressure-related diseases its role in mechanotransduction is not well understood. Here, we investigated how alterations in membrane cholesterol levels impact activation of TRPV4 (transient receptor potential vanilloid isoform 4), a stretch-activated cation channel, in trabecular meshwork (TM) cells that control intraocular pressure in the mammalian eye. Human TM cells responded to pharmacological depletion of free membrane cholesterol with augmented TRPV4 activation by agonist GSK1016790A, swelling and strain, and by increased membrane expression of TRPV4 immunoreactivity. Cyclic stretch increased the membrane cholesterol/phosphatidylcholine ratio and upregulated expression of F-actin, with the low-cholesterol effects reversed by cholesterol supplementation. Cholesterol depletion induced a constitutive current in TRPV4-expressing *Xenopus laevis* oocytes and obviated its activation by hypotonic swelling. Taken together, these findings suggest that cholesterol regulates translocation and activation of TRPV4, and guides its participation in macromolecular complexes, cytoskeletal architecture and cell-matrix contacts; in turn membrane cholesterol levels are dynamically regulated by the biomechanical milieu. By regulating TM pressure sensitivity, calcium homeostasis and contractility, cholesterol-TRPV4 interactions could influence IOP homeostasis and its role in glaucoma and diabetes.

Keywords: Cell signaling, cyclodextrins, dyslipidemias, eye/retina, glaucoma, lipid rafts, mechanotransduction, smooth muscle cells, TRPV4

Introduction

Cellular conversion of sensory information into electrical and chemical signals is uniquely constrained by unesterified cholesterol, a planar 27-carbon polycyclic lipid that constitutes ~20% of total mass of membrane lipids (1, 2). Intercalation of cholesterol into phospholipids reduces the motion of their hydrocarbon chains, affects the surface charge and promotes membrane stiffness while keeping the membrane fluid (3-5). Cholesterol regulates stereospecific interactions with transmembrane channels, transporters and enzymes within membrane-bound glycosphingolipid-rich protein complexes (lipid rafts; 6) that serve as organizing hubs for intracellular signaling pathways, membrane trafficking, cytoskeleton and cell-extracellular matrix (ECM) interactions in vertebrate cells and serves as a precursor for steroid hormones (1, 2, 7, 8). Alterations in free membrane cholesterol and lipid raft density tend to provoke a multiplicity of positive and negative effects on membrane channels, with little consensus about the molecular mechanisms (9 - 11).

Cholesterol levels within cells are maintained within a narrow range, with deficits or oversupply deleterious for health (5, 6). Defects in cholesterol regulation contribute to atherosclerosis, myocardial injury, diabetic and vascular dysfunctions (12 - 14) and increase the risk for progression of neurodegenerative diseases such as primary open angle glaucoma (POAG), a prevalent blinding disease (15, 16). Patients with high levels of serum cholesterol have increased likelihood for elevated IOP, with POAG linked to several genes involved in cholesterol metabolism (e.g., *ABCA1*, *CAV1*, *ARHGEF12*, and *DGKG)* (17, 18)). IOP is dynamically regulated by the trabecular meshwork (TM), a multilayered tissue composed of smooth-muscle-like cells with mechanosensitive and contractile properties (16, 19 - 21). TM stiffness and the phospholipid composition are altered in mice and humans with glaucoma (22,

23) and it would therefore be useful to obtain insight into how the biomechanical milieu impact TM lipids and whether changes in membrane cholesterol affect mechanotransduction.

We recently identified the mechanosensitive TRPV4 (Transient Receptor Potential Vanilloid 4) channel as a principal regulator of mechanically induced signaling in mouse and human TM (20, 24, 25). This ubiquitous nonselective cation channel transduces membrane strain, shear flow, swelling, temperature and polyunsaturated fatty acids into calcium signals (21, 24, 26, 27). Its sequence appears to have co-evolved with enzymes linked to cholesterol biosynthesis pathways (28) and studies in endothelial cells suggested that TRPV4 is trafficked to cholesterol- and caveolin1-enriched rafts (29). The objective of this study was to determine the mechanistic link between mechanotransduction, TRPV4 signaling and cholesterol in human TM cells and in an oocyte overexpression system. We found that manipulation of free membrane cholesterol profoundly affects TRPV4 sensitivity to mechanical stressors, calcium homeostasis and TM cytoarchitecture, and that lipid composition of the TM membrane is itself dependent on the history of mechanical stress, implicating cholesterol in homeostatic regulation of threshold sensitivities of TM mechanotransduction and cytoskeletal organization. A possible implication of our findings is that changes in systemic and/or local unesterified cholesterol levels affect TM sensitivity to IOP stress and capacity for homeostatic adjustment, and thereby influence the risk for contracting glaucoma.

Results

Reduction in free membrane cholesterol is associated with differential upregulation of ion channels

Unesterified cholesterol in primary TM cells isolated from healthy donors was visualized with filipin, a fluorescent indicator of cholesterol-binding. Cells were phenotyped by morphology, marker expression, responsiveness to corticosteroids (see Methods) and functional responses to TRPV4 agonists. Filipin, a naturally fluorescent polyene antibiotic that binds endogenous unesterified cholesterol (30) labeled discrete membrane and cytosolic domains (Fig. 1A-C) that presumably reflect lipid rafts (31). 60 min incubation with methyl-beta-cyclodextrin (MβCD; 10 mM), a water-soluble cyclic oligosaccharide that encapsulates hydrophobic membrane cholesterol residues and extracts cholesterol from the outer leaflet (32), reduced mean filipin fluorescence by 75.63% ± 2.77% ($P < 0.0001$) (Fig. 1B). Despite the near-complete removal of membrane cholesterol, cyclodextrin-treated cells remained viable and continued to respond to physiological stimuli over the duration of a typical experiment (~1-3 hours) (Figs. 6-7). Cholesterol:MβCD supplementation (1:10), which produces rapid and effective delivery of cholesterol to the plasma membrane (33), produced a striking increase in the number of filipin-positive puncta (6.17 ± 0.67; Fig. 1C & D). The efficacy of cholesterol depletion and enrichment effects on filipin signals suggest that cholesterol controls the formation of organized raft domains within the TM plasma membrane.

---Figure 1 near here---

Reduction in free membrane cholesterol is associated with upregulation of expression of F-actin signals

Mechanical stability of cells is maintained by interactions between the cell membrane, the cytoskeleton and the ECM. Cortical actin (arrowheads in Fig. 1) and ventral stress fibers (arrows) provide structural integrity and mediate cell – ECM contacts and contractility in unstimulated TM cells but may be reinforced in response to mechanical stress (19, 25, 34). Because cytoskeletal architecture reflects mechanical stresses associated with the TM membrane (24, 35) we asked whether changing its stiffness via cholesterol depletion/enrichment protocols impacts on the cytoskeleton. Cells were exposed to MβCD for 1 hour, fixed and labeled with phalloidin-actin Alexa 488. As shown in Figure 1A-C, loss of filipin staining was associated with significant increases in stress fiber fluorescence. The effect was dose-dependent, with 55.8 + 9.5% facilitation of F-actin observed in 10 mM cyclodextrin (Fig. 1B & D) ($N = 4$; $P < 0.001$). Supplementation with saturated 1:10 (1 mM) mixture of cholesterol and MβCD did not affect actin upregulation (Fig. 1C & E) despite the sizeable increase in the number of filipin^{+} puncta (Fig. 1C &D). This suggests actomyosin is not regulated by the lipid rafts themselves and/or that cholesterol levels in 'resting' TM cells may be close to saturation.

Chronic depletion of cholesterol facilitates agonist-induced TRPV4 activation

TRPV4 channels have emerged as central regulators of TM pressure, strain and volume sensing (20, 24), and were implicated in Ca^{2+}-dependent regulation of TM contractility and IOP (24, 25). Their association with lipid rafts (29) suggests potential susceptibility to changes in local cholesterol content. To test this, cells were loaded with the Ca^{2+} indicator dye Fura-2-AM and stimulated with the selective TRPV4 agonist GSK1016780A (GSK101) before and following 1 hour treatment with MβCD. As shown previously (24, 25), 25 nM GSK101 produced increases in $[Ca^{2+}]_i$ that gradually returned to baseline following washout (Fig. 2A). MβCD had no effect

on baseline $[Ca^{2+}]_i$ but increased peak amplitude of GSK101-evoked $[Ca^{2+}]_i$ elevations from 0.5 ± 0.04 (n = 39; N = 6) to 1.06 ± 0.13 (n = 53; N = 6; P < 0.0001) (~100% increase). Agonist stimulation under cholesterol-enriched conditions resulted in a small significant increase in the average calcium response to GSK101 (0.74 ± 0.05; n = 44; N = 5; P < 0.001).

Fig. 2A-B show Ca-imaging data from single cells but we also employed spectrophotometry to assess the effects of cholesterol depletion on the population response of Fluo-4 AM -loaded cells. 5 nM GSK101 produced a 24.8% ± 8.31% increase in the fluorescence signal (N = 4 independent experiments; P < 0.05; Supplementary Fig. 1A). MβCD produced an additional ~ 12% increase, resulting in 36.27% ± 5.18% increase compared to the baseline (P < 0.05) (Fig. 2C). A similar facilitatory effect was observed with 25 nM GSK101 (Supplementary Fig. 1A). These data suggest that association with lipid rafts suppresses TRPV4 activation.

---Figure 2 near here---

Cholesterol modulates swelling -induced calcium signaling

Originally identified as a regulator of cellular swelling (36, 37), TRPV4 functions as a real-time readout of cell volume changes (38) with osmoregulatory functions in neurons, glia, epithelial and endothelial cells (39 - 44). To determine the effect of raft disruption on the TM swelling response, we exposed the cells to hypotonic stimuli (HTS) in the presence/absence of MβCD. Consistent with TRPV4 activation, TM cells responded to 140 mOsm HTS with significant (0.44 ± 0.06 Y; n = 24; N = 4; P < 0.0001) increases in $[Ca^{2+}]_i$ (Fig. 3A & B). Depletion of cholesterol approximately doubled

the peak response amplitude to 0.87 ± 0.08 (n = 27; N = 4; P < 0.001), with the facilitatory effect inhibited by cholesterol supplementation (0.43 ± 0.04; n = 30; N = 4; P < 0.001) (Fig. 3A & B). Spectrophotometry similarly showed dose-dependent $[Ca^{2+}]_i$ increases in response to HTS (in case of 55% HTS: 1.14 ± 0.03; N = 3), and augmentation by cholesterol removal (to 1.21 ± 0.022; N = 3) (Fig. 3C & Supplementary Fig. 1B) (P < 0.05).

---Figure 3 near here---

Cholesterol modulates the TM response to membrane strain

We then asked whether cholesterol depletion impacts on transduction of cyclic mechanical stretch, which represents an important feature of IOP-induced biomechanical stress impelled on ECM beams that support TM cells (45 - 47) and was shown to involve TRPV4 (24, 25). Cells were seeded onto elastic silicone membranes of a StageFlexer device and stimulated with periodic, calibrated displacements/ relaxations of the collagen IV–coated substrate (1 Hz; 10% elongation, 15 minutes). Cyclic stretch evoked uniform and reversible elevations in cytosolic $[Ca^{2+}]_i$ to 0.21 ± 0.02 (n = 21; N = 6; P < 0.0001), an effect that was augmented by cholesterol depletion to 0.71 ± 0.04 (n = 77; N = 5; P < 0.0001) and reduced by cholesterol supplementation to 0.38 ± 0.05 (n = 37; N = 6; P < 0.0001) (Fig. 4A & B).

TRPV4 channels were proposed to regulate trabecular contractility and outflow via the modulation of TM actomyosin (24). Stretch and cholesterol depletion upregulate TM F-actin expression (Fig. 1) but it would be important to

know if stretch-dependence of actin remodeling is itself cholesterol-dependent. To test this hypothesis, cells were exposed to cyclic (0.5 Hz) 6% stretch in the presence/absence of MβCD. 1 hour of stretching augmented phalloidin-actin fluorescence (1.32 ± 0.05; N = 3; P < 0.001; Fig. 5A panel ii & C) but significantly reduced the density of filipin puncta (0.76 ± 0.05; N = 3; P < 0.01; Fig. 5A panel ii & B), indicating that lipid rafts and the actin cytoskeleton are sensitive to the ambient mechanical stress (Fig. 4). As shown in Figure 1, MβCD increased cortical and stress fiber signals (1.56 ± 0.09; N = 3; P < 0.0001), and reduced the density of filipin (0.24 ± 0.03; N = 3; P < 0.0001). While stretch does not further decrease filipin fluorescence in MβCD-treated cells (0.26 ± 0.02; N = 3) (Fig. 5A, panels iii, iv & B), stress fiber fluorescence showed a significant 42.6% ± 21.6% increase over the effect of stretch alone (N = 3; P < 0.05). These findings suggest that membrane cholesterol content regulates the stretch-dependence of cytoskeletal remodeling.

----Figures 4 & 5 near here---

Membrane cholesterol regulates TRPV4 expression

Depending on the cell type and protein isoform, cholesterol-modulating agents potentiate or inhibit TRP channel trafficking (48 - 50). To determine the effect of membrane cholesterol manipulations on channel expression, cells were fixed and labeled with a validated anti-TRPV4 antibody (Jo et al., 2015; Lakk et al., 2018). 1 hour incubation with MβCD produced a 4.49 ± 1.07-fold increase in the number of TRPV4-ir puncta (N = 3; P < 0.05). Cholesterol enrichment

abrogated this effect (0.73 ± 0.28; N = 3; P < 0.05; Fig. 6), suggesting that membrane cholesterol suppresses TRPV4 translocation.

---Figure 6 near here-----

TRPV4 current in heterologously expressing oocytes is potentiated by MβCD

The opening of the TRPV4 channel pore in mammalian cells reflects a multitude of simultaneous inputs that include mechanical stressors, temperature, polyunsaturated fatty acids and accessory binding proteins (43, 51, 52). To isolate the effects of cholesterol on the channel from auxiliary proteins and intracellular signaling within TM cells, we determined the cholesterol-dependence of TRPV4 currents in the *Xenopus laevis* expression system that has been previously used to study the effects of cholesterol depletion (53) and TRPV4 signaling (38, 40, 44). Because oocyte viability is compromised at mM MβCD concentrations (53), the experiments were conducted using 50 μM MβCD.

Membrane currents in uninjected control oocytes and TRPV4-expressing *Xenopus* oocytes were monitored by conventional two-electrode voltage clamp. A voltage step protocol demonstrated small tonic currents in TRPV4-expressing oocytes (Fig. 7A, upper left panel) compared to those obtained in uninjected oocytes (Fig. 7A, lower left panel), summarized data in Fig. 7B and inset. While the transmembrane currents of uninjected oocytes were undisturbed by addition of MβCD exposure (Fig. 7A lower right panel and Fig. 7B inset), those of the TRPV4-expressing oocytes were enhanced approximately 10-fold (Fig. 7A upper right panel and Fig. 7B) by cholesterol depletion, compare 156 ± 42 nA with 1466 ± 475 nA, N = 9, P = 0.014, Fig.

7B inset. These data indicate that membrane cholesterol suppresses tonic TRPV4 activity, with depletion thereof enhancing the TRPV4-mediated membrane currents.

---Figure 7---

Tensile stretch regulates the relative expression of membrane lipids

The mechanical properties of the lipid bilayer can change under tension (54), but it is not known if the lipid content of the membrane is itself shaped by biomechanical milieu. We thus tested whether changing the mechanical properties of the membrane is sufficient to alter its cholesterol content and the C/P (cholesterol/phosphatidylcholine) molar ratio. TM cells were stretched (0.5 Hz; 6% elongation) for 1 and 3 hours, cells were lysed, and the extracted lipids examined with phosphatidylcholine (PC) fluorometric assay and GS/MS. The data was normalized relative to unstimulated controls calibrated with standards (PC or cholesterol). Stretch produced a striking time-dependent decrease in membrane cholesterol content to 0.58 ± 0.089 (1 hour; N = 3; $P < 0.01$) and 0.30 ± 0.02 (3 hours; N = 3; $P < 0.001$) (Fig. 8A & B). This was accompanied by increases in membrane content of PC to 1.32 ± 0.02 (1 hour; N = 3; $P < 0.0001$) and 1.58 ± 0.03 (3 hours; N = 3; $P < 0.01$) (Fig. 8C). These results demonstrate that the C/P ratio is sensitive to the mechanical strain. Thus, the mechanical properties and function of the TM membrane might reflect the history of its exposure to mechanical stress.

----Figure 8---

Discussion

In this study we examined how mechanical properties of the lipid bilayer control signaling by a ubiquitous mechanically gated channel, determined the impact of TRPV4-cholesterol interaction on TM cells' cytoarchitecture and then confirmed the effects of cholesterol depletion on mechanically induced TRPV4 activation in heterologously expressing cells. The key findings are (i) Membrane cholesterol and lipid rafts negatively modulate TRPV4-dependent mechanosensitivity; (ii) Expression of F-actin (which tends to be proportional to cell stiffness and contractility (55) is cholesterol- and stretch-dependent; (iii) TM membrane lipid content is regulated by physiological levels of cyclic mechanical stretch, and (iv) Cholesterol tonically suppresses TRPV4 activation in heterologously expressing cells. These findings suggest that cholesterol metabolism and trafficking could play a role in homeostatic regulation of mechanotransduction, calcium homeostasis and cytoskeletal signaling.

We demonstrate that the cholesterol content of TM membranes reflects a feedback loop between mechanical stress and activation of intrinsic mechanotransduction mechanisms. Mechanical strain dynamically regulates the C/P ratio and cholesterol levels within the membrane and vice versa, cholesterol levels regulate the cells' susceptibility to mechanical stressors such as HTS and tensile stretch. Cholesterol depletion was visualized as near-total dissolution of membrane filipin fluorescence that presumably reflected the loss of lipid rafts and correlated with increased calcium signaling evoked by GSK1016790A, cyclic strain and cell swelling. MβCD-induced potentiation of TRPV4 activation was observed in single cells and cell populations, and confirmed in a recombinant system that showed constitutive activation of transmembrane currents in TRPV4-expressing, but not control, oocytes. These findings suggest that cholesterol functions as a negative regulator of TRPV4 signaling in TM cells and in the

Xenopus laevis expression system. Facilitation of TRP currents by MβCD has been previously reported for TRPM8 (48), TRPM3 (49), TRPC3 isoforms (56) and volume-activated chloride (VRAC) channels (57). Although MβCD is not a physiological modulator, another cholesterol scavenger, the oxidized low-density lipoprotein (oxLDL), appears to have similar effects on cellular biomechanics (58). Supplementation with exogenous MβCD:cholesterol produced ~6-fold increase in the number of putative lipid rafts (Figure 1) and obviated the facilitation by MβCD without affecting peak amplitudes of agonist- and mechanically-evoked calcium signals. This might be indicative of saturation of control membranes with free cholesterol, which constitutes ~third of lipid mass with 75-80% cholesterol distributed to the inner bilayer leaflet (5, 33). It is worth noting that cholesterol enrichment does not affect lateral diffusion of membrane lipids or proteins (59. 60) and that, in contrast to the effects of MβCD, MβCD:cholesterol micelles do not affect the gating of mechanosensitive Piezo1 channels (61).

If cholesterol regulated ion channels principally by altering the bulk mechanical properties of the membrane, its effects should be translatable across experimental systems yet in contrast to our observations in TM cells, MβCD *suppresses* TRPV4 activation in retinal glia (62), inhibits TRPV4-mediated Ca^{2+} influx in mesenteric endothelial cells (29), reduces TRPA1, TRPC1, TRPC6 activation in mammalian cells (63 - 65), and blocks TRPL currents in fly photoreceptors (66). Visoelastic "force-from-lipid" models (54, 67, 68) cannot explain why cholesterol enantiomers with similar effects on membrane properties have dramatically different effects on channel function (69). The range of cholesterol effects on TRPV4 and ion channels in general (11) favors allosteric models in which cholesterol binds to channel subunits, accessory proteins at the protein-lipid interface and/or residues buried within the bilayer. Cholesterol molecules may adopt a variety of poses within the TRP channel domains (70) to control

modality-specific responsiveness to the lipid milieu, as suggested by the differential modulation of TRPV4 signaling in TM and glia. Consistent with this, TRPV4 activity in yeast (which cannot synthesize cholesterol) can be induced by swelling but not temperature (71). The cognate TRPV1 channel shows comparable context-dependence, with MβCD inhibiting capsaicin- and proton-evoked currents in sensory neurons (72, 73) and facilitating thermal sensitivity of TRPV1 currents in HEK293 cells (72) whereas cholesterol enrichment had a strong suppressive effect in excised patches, which do not experience protein trafficking (50). By analogy with TRPA1, which preferentially localizes to cholesterol-rich domains and employs the Cholesterol Recognition/Interaction Amino acid Consensus (CRAC) motif for raft interactions (74), MβCD-induced changes in bilayer tension could disrupt hydrogen bonds between TRPV4 residues to modulate the opening of the channel gate (75) or disinhibit CRAC-like (KDLFRFLL) recognition motifs that span Loop 4 – TM5 of TRPV1/4 (28, 76).

TRPV4-ir in TM cells manifests as puncta of varying size that presumably correspond to clustering of TRPV4 proteins. The ~4.5-fold increase in the number and intensity of the puncta (Figure 6) implicates cholesterol in the regulation of transport and/or retrieval of TRPV4-containing vesicle pools, possibly via PACSIN that binds the N-terminus (77) or SNARE proteins (78). MβCD was shown to regulate trafficking of Kv1.5 (77), Kir (78), LRRC8/SWELL (57) and TRPC3 (56) channels, with both MβCD and mutations in cholesterol-binding residues reducing the membrane density of TRPV1 channels/current (50, 79).

Another interesting observation concerns stretch-dependent plasticity of TM membrane lipids, which manifested as reduction in the C/P ratio following exposure to physiological levels of cyclic stretch. This novel effect was inhibited by HC067047, suggesting that TRPV4-mediated transduction of strain modulates the material properties of membrane lipids. A reduction in the

C/P ratio might represent a protective response that allows cells to dynamically reduce stiffness in the presence of mechanical stress. In contrast, increased C/P ratios that were reported in glaucomatous TM cells (22) could indicate compromised capacity for homeostatic adjustments. It remains to be seen to what extent TRPV4 activation (and/or calcium) contributes to the transitions between pools of membrane cholesterol, i.e., sequestered or chemically inactive vs. 'accessible' (i.e., unsequestered or chemically active) pools. The sensitivity of TM mechanotransduction to cholesterol modulation and C/P ratio adjustment in the presence of cyclic stretch suggest that healthy cells experience a dynamic interplay between the lipid milieu, intracellular calcium and cytoskeletal organization that is perturbed by altered membrane cholesterol levels.

Interaction between the cell membrane and the cytoskeleton has major impact on mechanosensing and cell function. Pressure-sensitive stiffening of TM cells and increased contractility of their actomyosin appear to underlie increased tissue resistance to fluid outflow (Rao et al., 2017; Vahabikashi et al., 2018). While upregulation of F-actin in response to membrane stretch (Figure 5) accords with previous observations of its TRPV4-dependence (19, 25), its sensitivity to cholesterol depletion indicates that TM cytoarchitecture could be influenced by both dynamic (stretch) properties of the membrane and its lipid composition. Similar effects of MβCD on actin polymerization and cell contractility were reported in osteoblasts, endothelial cells, tumor cells and myocytes (80 - 82). How membrane cholesterol regulates the cytoskeleton is not understood, with possibilities including binding to raft domains or regulation of adhesion energy between actin monomers and the membrane (83).

Studies of the conventional outflow pathway suggest that aqueous humor outflow is fine-tuned by both lipid rafts and TRPV4 channels. Caveolin-1, which binds free cholesterol and

functions as negative regulator of signal transduction within the raft (84), was shown to suppress trabecular outflow (85, 86). Statin inhibitors of HMG-CoA reductase were reported to mitigate cholesterol-associated changes in aqueous outflow and IOP elevations (87), and polymorphisms at *CAV1/2* gene loci were linked to both POAG and IOP (88, 89) whereas topical, intraocular and systemic exposure of the eye to TRPV4 antagonists produced significant IOP lowering (24). The role of cholesterol in transduction of mechanical stressors thus represents a mechanism that could contribute to dysfunctional mechanosensory signaling associated with glaucoma, diabetic retinopathy and other neuropathic diseases.

2. MATERIALS AND METHODS

TM cell culture and isolation. Primary cultures of TM (pTM) cells were dissected from 3 eyes of donors with no history of eye disease (65-year-old male, 68-year-old male, 78-year-old male) as described previously (24, 25, 90) and in concordance with the tenets of the WMA Declaration of Helsinki and the Department of Health and Human Services Belmont Report. A subset of experiments was conducted in immortalized juxtacanalicular human trabecular meshwork (hTM cells) obtained from ScienCell (Catalog#6590) and used up to the 7th passage. pTM and hTM cells showed no differences in responses to TRPV4 or cholesterol-modulating agents. Cells were grown in Trabecular Meshwork Cell Medium (TMCM, ScienCell, Catalog#6591) at 37 °C and 5% CO_2. The phenotype was periodically validated by profiling for markers, including *Aqp1*, *Timp3*, *Myoc*, *MGP*, *Acta2* (α-smooth muscle actin, αSMA) and dexamethasone-induced upregulation of myocilin expression. These data are shown in our previous characterizations of the cell line (21, 24, 90).

Xenopus laevis oocyte experiments were performed according to the guidelines of the Danish Veterinary and Food Administration (Ministry of Environment and Food), and approved by the animal facility at the Faculty of Health and Medical Sciences, University of Copenhagen. The experiments conform to the principles and regulations described in (91). The surgical protocol by which the oocytes were retrieved was approved by The Danish National Committee for Animal Studies, Danish Veterinary and Food Administration (Ministry of Environment and Food). An abstract version of this work appeared in (92).

Reagents. The TRPV4 agonist GSK1016790A (GSK101) and cholesterol were obtained from Sigma or VWR. GSK101 (1 mM) stock aliquots were prepared in DMSO and subsequently diluted into working saline concentrations (5 and 25 nM, respectively). Chemical reagents for biochemical experiments - methanol, isopropanol, n-hexane, and chloroform - were of GC/MS grade and purchased from Fisher Scientific. The cholesterol standard was purchased from Sigma-Aldrich.

Cholesterol depletion and repletion. Methyl-β-cyclodextrin (MβCD; Sigma C4555) was dissolved in TMCM and used at 10 mM, the concentration that removes 80-90% of free membrane cholesterol (32, 33). Cells were preincubated with MβCD for 60 min to maximize extraction, washed in TMCM and placed into recording chambers for optical recordings. This protocol maintains decreased membrane cholesterol levels for at least 24 hours (78). Supplementation was based on perfusion with cholesterol-saturated MβCD. Powdered cholesterol was dissolved for 30 min in 80% ethanol solution at 75 - 80° C to obtain a 10 mM stock solution. The stock was dissolved in TMCM containing MβCD to obtain the final cholesterol concentration of 1 mM. A parallel chamber used the cholesterol stock to load MβCD for the final concentrations of 1 mM cholesterol + 10 mM MβCD.

Hypotonic stimulation. The swelling studies were conducted as reported previously (40, 44). Extracellular NaCl was kept at 57.5 mM and total osmolarity regulated by addition or removal of mannitol, a procedure that maintains the ionic strength of the extracellular solution. Osmolarity was checked thermometrically using a vapor pressure osmometer (Wescor).

Lipid extraction and GC-MS Chromatography . Lipids were extracted using Folch method (93). Total lipids were extracted by adding methanol/chloroform/water (1:2:1, v/v). The chloroform phase was washed to remove water residues and dried under nitrogen gas. The dried film was dissolved in 100 µl hexane and 5 µl of sample was injected into the GC-MS instrument for cholesterol analysis. The Thermo Trace GC-DSQ II system (ThermoFisher Scientific) consists of an automatic sample injector (AS 3000), gas chromatograph (GC), single quadrupole mass detector, and an analytical workstation. Chromatographic separation was carried out with an Rxi-5MS coated 5% diphenyl/95% dimethyl polysiloxane capillary column (30 m × 0.25 mm i.d, 0.25 µm film thickness) (Restek Corporation, PA). The sample was injected into the GC/MS using a splitless mode, the septum purge was on, and the injector temperature was set at 200°C. The column temperature was programmed as follows: initial temperature 60°C, 15 degrees/min to 240°C, 2 degrees/min to 290°C, and a hold at 290°C for 5 min. Transfer line temperature was 290°C. Helium was used as the carrier gas at a flow rate of 1.5 ml/min. MS conditions were as follows: electron ionization mode with ion source temperature of 250°C and multiplier voltage, 1,182 V; full scan and selected ion monitoring (SIM) mode was used for the identification and quantification of cholesterol. The area values of cholesterol were plotted against known range of standards (100 to 0.1 ng) to quantify the cholesterol in the samples. Phosphatidylcholine levels were measured by a colorimetric/fluorometric assay kit (BioVision).

Immunofluorescence. Cells were fixed with 4% paraformaldehyde for 10 min. After a PBS rinse, PBS containing 5% FBS and 0.3% Triton X-100 blocking solution was applied for 20 minutes. F-actin was labeled with AlexaFluor 488 phalloidin (1:1000, Life Technologies). Primary antibody (rabbit polyclonal anti-TRPV4; 1:1000; Lifespan Biosciences) was diluted in antibody solution (2 % BSA, 0.2 % TritonX-100 in PBS) and applied overnight at 4°C. After rinsing, slices were incubated with secondary antibodies diluted to 1:1000 in PBS for one hour at RT. Plasma membrane cholesterol was tracked with filipin (Sigma F9765) as previously described (62). 0.005% filipin (Sigma) dissolved in DMSO and applied to dissociated cells together with the secondary antibody (goat anti-rabbit AlexaFluor 488; 1:500; Life Technologies). Unbound antibodies were rinsed and conjugated fluorophores protected with Fluoromount-G (Southern Biotech) prior to coverslipping. The TRPV4 antibody does not label TRPV4 KO tissues (94, 95). Images (10 per experiment) were acquired on Olympus CV1200 confocal microscope using a NeoFluor 20x water immersion objective.

Immunofluorescence analysis and particle counting. Images were acquired using identical parameters (HV, gain, offset) resulting in very similar signal-to-noise ratios across datasets. ImageJ was used to extract and quantify the mean intensities and particle analysis of immunoreactive signals, with ~40-50 cells per slide averaged across at least 3 independent experiments. Color images were converted to black and white using *Binary→Convert to mask* with white background and automatic threshold level. Immunoreactive puncta (number/cell area) with the segmented area were counted with the *Analyze particles* plug-in. Minimum (3 pixel^2) and maximum (30 pixel^2) pixel area sizes were defined to exclude areas outside of the ROI, calculate the particle number/cell area and determine the relative particulum numbers. Individual particulum sizes for each cell were averaged and normalized.

Optical Imaging. Calcium responses in TM cells were tracked following published protocols (94, 96). Briefly, for CCD imaging, cells were loaded with 5-10 µM Fura-2-AM for 45 min and perfused with isotonic saline (pH 7.4) containing (in mM): NaCl 133, KCl 2.5, NaH_2PO_4 1.5, $MgCl_2$ ($6H_20$) 1.5, $CaCl_2$ 2, glucose 10, HEPES hemisodium salt 10, pyruvic acid 1, lactic acid 1, L-glutamine 0.5, glutathione 0.5, Na-ascorbate 0.3, with pH 7.4 and osmolarity at 300 ± 10 mOsm, delivered through a gravity-fed 8-reservoir system (Warner Instruments) that converged towards a manifold tube inserted into the experimental chamber. Epifluorescence was detected with Photometrics Delta or Prime BSI cameras. Ratiometric Ca^{2+} imaging was performed on Regions of Interest (ROI) that marked a central somatic region, and were typically binned at 3x3 (95, 97). Background fluorescence was measured in similarly sized TM ROIs in neighboring areas devoid of cells. The microscopes were inverted Nikon Ti with 40x (.75 NA oil) or upright Nikon E600 FN microscopes with a 20x (0.8 NA water) and 40x (1.3 N.A. oil & 0.8 N.A. water) objectives. A wide-spectrum 150W Xenon arc lamp (DG4, Sutter Instruments, Novato, CA) provided excitation to 340 nm and 380 nm filters (Semrock). The signals were analyzed using NIS-Elements AR 3.2 and MS Excel ΔR/R (peak F^{340}/F^{380} ratio – baseline/baseline) was used to quantify the amplitude of Ca^{2+} signals. Data acquisition and F340/F380 ratio calculations were performed by NIS Elements 3.22 software (Melville, NY).

Spectrophotometry. $[Ca^{2+}]_i$ was monitored using a plate reader (Turner Biosystems). Cells were seeded onto non-coated 96-well plates and loaded with 2 uM of Fluo-4 AM for 30-45 min at 37 □C. Fluorescence was measured at 490 nm excitation and 520 nm emission, with 90 sec intervals, and 6-10 measurements per experiment. 490/520 nm ratios were normalized to the control untreated samples. Baseline measurements were recorded in control wells at the same time withoutaddition of agonist or HTS.

Membrane strain assay. TM cells were seeded on flexible silicon membranes coated with type I/IV collagen, grown to 80% confluence and placed into a FlexJunior chamber controlled by the Flexcell-5000 Tension system (Flexcell) (24). For determination of stretch-induced Ca^{2+} influx and cytoskeletal changes, cells were loaded with Fura-2-AM for 30-60 minutes and stimulated with cyclic biaxial stretch (10%, 1Hz, 15 min, or 6%, 0.5Hz 1-3 hours; respectively)at 37 □C. A 15 minute stretch period was chosen to optimize capture of the stretch-evoked fluorescent response by adjusting for the change in focal plane (which disrupted calcium imaging for several seconds as indicated by breaks in response trace in Fig. 4A). Cells were imaged with a Nikon E600FN upright microscope. Excitation light was provided by a Xenon source within a Lambda DG4 (Sutter Instruments) and controlled by Nikon Elements.

RNA preparation and heterologous expression in Xenopus laevis oocytes. Xenopus laevis frogs were obtained from Nasco (Fort Atkinson). The frogs were kept in tanks in a recirculating water facility, and fed twice weekly with Floating Frog Food 3/32 for adults and juveniles (Xenopus Express, Inc.). Oocytes were surgically removed from anesthetized frogs (38, 44) under anesthesia (2 g/L Tricain, 3-aminobenzoic acid ethyl ester, Sigma A-5040). Preparation of defolliculated oocytes was carried out as described in (98). Oocytes were kept in Kulori medium (in mM): 90 NaCl, 1 KCl, 1 $CaCl_2$, 1 $MgCl_2$, 5 HEPES (pH 7.4). cDNA encoding rat TRPV4 was subcloned into the oocyte expression vector pXOOM, linearized downstream from the poly-A segment, and *in vitro* transcribed using T7 mMessage machine according to manufacturer's instructions (Ambion). cRNA was extracted with MEGAclear (Ambion) and microinjected into defolliculated *Xenopus laevis* oocytes: 4 ng TRPV4 RNA/oocyte. A TRP channel antagonist, Ruthenium Red (1 μM, Sigma Aldrich, R-2751) was added to the medium to prevent the tonic

TRPV4-mediated currents mediating oocyte lysis. The oocytes were kept for 3-4 days at 19˚C prior to experiments.

Electrophysiology and volume recordings of oocytes. Conventional two-electrode voltage clamp studies were performed with a DAGAN CA-1B High Performance oocyte clamp (DAGAN) with Digidata 1440A interface controlled by pCLAMP software, version 10.5 (Molecular Devices) (44). Electrodes were pulled (HEKA, PIP5) from borosilicate glass capillaries to a resistance of 2.5-3 MΩ when filled with 1 M KCl. Current traces were obtained by stepping the clamp potential from -20 mV to test potentials ranging from +50 mV to -130 mV (pulses of 200 ms) in increments of 15 mV. Recordings were low pass-filtered at 500 Hz, sampled at 1 kHz, and the steady-state current activity was analyzed at 140-180 ms after applying the test pulse. Oocytes were placed in an experimental recording chamber, perfused, and volume measurements were performed as described (38). Briefly, oocytes were placed in a small chamber with a glass bottom and perfused with solutions of interest. The cell volume was viewed from below via a long-distance objective, and micrographs captured continually at the rate of 25 images/sec. HTS used to induce cell swelling consisted of (in mM): 50 NaCl, 2 KCl, 1 $MgCl_2$, 1 $CaCl_2$, 10 HEPES, 100 mM mannitol (Tris buffered pH 7.4, 220 mOsm), with the hypotonic solution made by removing mannitol. Osmolarity was verified to an accuracy of 1 mOsm with an osmometer (Type 15; Löser Messtechnik). 100 μM Ruthenium Red (dissolved in water to a stock of 1 mM and kept at -20 °C) was applied to suppress TRPV4 activity. Depletion of endogenous cholesterol in intact oocytes was induced with 50 μM MβCD for 45 min (e.g., 50). All experiments were performed at room temperature (23 °C).

Data Analysis. Statistical analyses were performed with GraphPad Prism 6.0 and Origin Pro 8.5. Data was acquired from at least three different experimental preparations on different days, with

3-6 slides/experiment. Typically three different batches of oocytes were used. Unless indicated otherwise, unpaired or paired t-tests were used to compare two means, and a one-way ANOVA along with the Tukey's test was used to compare three or more means. Means are shown ± SEM. $p > 0.05$ = NS, $p < 0.05$ = *, $p < 0.01$ = **, $p < 0.001$ = *** and $p < 0.0001$ = ****.

Data Availability. The data described in the mansucript are contained within the manuscript.

FIGURE LEGENDS

Figure 1 – Cholesterol depletion promotes formation of actin stress fibers. Double-labeling for F-actin (phalloidin-Alexa 488 nm) and filipin (405 nm). (A) Untreated preparations show typical stress fiber organization dotted by lipid rafts. (B) 1-hour incubation with MβCD results in dissolution of filipin^{+} puncta and upregulation of phalloidin-actin fluorescence. (C) Saturated 1:10 admixture of cholesterol (1 mM) and MβCD (10 mM) increased the number of filipin puncta. (D-E) Averaged data for experiments shown in A-C (N = 3-4). Scale bar: 50 µm. *, $P < 0.05$, **; $P < 0.01$, ***, $p < 0.001$ and ****, $p < 0.0001$.

Figure 2 – Cholesterol depletion increases the amplitude of TRPV4 agonist-induced Ca^{2+} signals. (A-B) Ratiometric signals in Fura-2 AM-loaded cells. (A) GSK101-induced elevations are increased in MβCD -treated cells (n = 8-10) (B) Averaged data. MβCD (blue bar) augmented, whereas MβCD:cholesterol (green bar) reduced the amplitude of agonist-induced fluorescence. (C) Fluorimetry, cell populations in 96 wells. 5 nM GSK101 increased Fluo-4 fluorescence. Its effect was facilitated (~ 12%) by MβCD (N = 4). **, $P < 0.01$; ***, $P < 0.001$; ****, $P < 0.0001$; N.S., non-significant.

Figure 3 – Cholesterol depletion facilitates HTS-induced Ca^{2+} signals. (A-B) Cytosolic Ca^{2+} responses in Fura-2 AM-loaded cells. (A) HTS induced $[Ca^{2+}]_i$ elevations in representative control, MβCD and MβCD:cholesterol -treated samples (n = 8-10) (B) Averaged data from A. MβCD (blue bar) augmented, whereas MβCD:cholesterol (green bar) reduced HTS-induced $[Ca^{2+}]_i$ increases. (C) Fluorimetry. 55% HTS (140 mOsm) increased Fluo-4 signals. This effect was facilitated by MβCD (N = 3). ***, P < 0.001; ****, P < 0.0001; N.S., non-significant.

Figure 4 – Membrane cholesterol modulates the cyclic stretch induced intracellular calcium responses in TM cells. (A) Representative traces and (B) Averaged results for 15 min cyclic stretch of control (black trace, bars), MβCD-treated (10 mM, blue trace, bar) and MβCD:cholesterol-treated (green trace, bar) TM cells. Stretch-evoked $[Ca^{2+}]$i responses are modulate by membrane cholesterol (n = 21-77; N = 5-6). ****, P < 0.0001.

Figure 5 – Membrane cholesterol content regulates stretch-dependence of cytoskeletal remodeling. TM cells were stretched in the presence/absence of MßCD and MßCD:cholesterol, and labeled for filipin and phalloidin-Alexa 488 nm. (A) Control cells. (B) 6% cyclic stretch (C) MßCD. (D) MßCD + Stretch. (E) Filipin fluorescence is significantly reduced by stretch and MßCD alone. (F) Both stretch and MßCD facilitate F-actin fluorescence. Combined stimulation results in additional xxx Stretch-induced increases in stress fiber fluorescence were facilitated by MßCD (10 mM). *, P < 0.05; **, P < 0.01; ***, P < 0.001; ****, P < 0.0001.

Figure 6 – Cholesterol depletion increases the number of TRPV4-ir puncta. TRPV4 immunolabeling of primary TM cells. (A) Control, (B) MßCD and (C) MβCD:cholesterol-treated

TM cells. (D) The number of TRPV4 particuli, normalized for control cells, is upregulated after 1 hour incubation with MßCD (N = 3). *, P < 0.05.

Figure 7 – Cholesterol depletion enhances TRPV4-mediated membrane currents in *Xenopus* oocytes (A) Representative current traces from TRPV4-expressing oocytes (top panels) and uninjected control oocytes (lower panels) in control solution (left panels) or after 45 min exposure to 50 µM MβCD (right panels). (B) I/V curves of TRPV4-expressing oocytes exposed to control solution or MβCD, with uninjected oocytes in inset. Summarized currents obtained at -85 mV demonstrated in lower inset. The magnitude of TRPV4-mediated currents (at V_m = -85 mV) were compared using Students *t*-test. **, P < 0.01; ns: not significant. *N* = 9.

Figure 8 –The C/P ratio in TM membranes is stretch-dependent. (A) Representative chromatograms and (B) Normalized and averaged cholesterol GS/MS data in control, 1 h and 3 hour stretched primary TM cells, (C) Normalized and averaged phosphatidylcholine (PC) fluorometric data in control, 1 h and 3 hour stretched primary TM cells. Stretch induced a time-dependent decrease in membrane cholesterol level, which was concomitant with increasing content of membrane PC. N = 3; **, P < 0.01; ****, P < 0.0001.

Supplementary Figure 1 – Averaged, maximum fluorescence data in Fluo-4 loaded TM cells. (A) Spectrophotometry shows dose-dependent $[Ca^{2+}]_i$ increases in response to 5 and 25 nM GSK and augmentation by cholesterol removal (N = 4) (B) Data shows dose-dependent $[Ca^{2+}]_i$ increases in response to different HTS solutions and augmentations by cholesterol removal (N = 3). *, P < 0.05.

Acknowledgements

We thank Dr. Amy Lin (Moran Eye Center, University of Utah) for corneal rims.

References

1. Yeagle, P.L. (1985) Cholesterol and the cell membrane. Biochim Biophys Acta 822, 267-87.
2. Pike, L.J. (2003) Lipid rafts: bringing order to chaos. J Lipid Res 44, 655-67.
3. Jamieson GA, Robinson DM (1977) Mammalian Cell Membranes, vol. 2. Butterworth, London
4. Lundbaek, J.A., Birn, P., Hansen, A.J., Søgaard, R., Nielsen, C., Girshman, J., Bruno, M.J., Tape, S.E., Egebjerg, J., Greathouse, D.V., Mattice, G.L., Koeppe, R.E., Andersen, O.S. (2004) Regulation of sodium channel function by bilayer elasticity: the importance of hydrophobic coupling. Effects of Micelle-forming amphiphiles and cholesterol. J Gen Physiol 123, 599-621.
5. Lange, Y., Steck, T.L. (2008) Prog Lipid Res 47, 319-32. Cholesterol homeostasis and the escape tendency (activity) of plasma membrane cholesterol.
6. Subczynski, W.K., Pasenkiewicz-Gierula, M., Widomska, J., Mainali, L., Raguz, M. (2017) High Cholesterol/Low Cholesterol: Effects in Biological Membranes: A Review. Cell Biochem Biophys. 75, 369-385.
7. Sezgin, E., Levental, I., Mayor, S., Eggeling, C. (2017) The mystery of membrane organization: composition, regulation and roles of lipid rafts. Nat Rev Mol Cell Biol. 18, 361-374.

8. Korade, Z., Kenworthy, A.K. (2008) Lipid rafts, cholesterol, and the brain. Neuropharmacology 55, 1265-73.
9. Mauch, D.H., Nägler, K., Schumacher, S., Göritz, C., Müller, E.C., Otto, A., Pfrieger, F.W. (2001) CNS synaptogenesis promoted by glia-derived cholesterol. Science 294, 1354-1357.
10. Marquer, C., Devauges, V., Cossec, J.C., Liot, G., Lécart, S., Saudou, F., Duyckaerts, C., Lévêque-Fort, S., Potier MC (2011) Local cholesterol increase triggers amyloid precursor protein-Bace1 clustering in lipid rafts and rapid endocytosis. FASEB J 251, 295-305.
11. Levitan, I., Barrantes, F.J. (2012) Cholesterol Regulation of Ion Channels and Receptors. John Wiley & Sons
12. Fliesler, S.J., Bretillon, L. (2010) The ins and outs of cholesterol in the vertebrate retina. J Lipid Res. 51, 3399-3413.
13. Brownell, W.E., Jacob, S., Hakizimana, P., Ulfendahl, M., Fridberger, A. (2011) Membrane cholesterol modulates cochlear electromechanics. Pflugers Arch. 461, 677-686.
14. Kacher, R., Lamazière, A., Heck, N., et al. (2019) CYP46A1 gene therapy deciphers the role of brain cholesterol metabolism in Huntington's disease. Brain 142, 2432-2450.
15. Jonas, J.B., Aung, T., Bourne, R.R., Bron, A.M., Ritch, R., Panda-Jonas, S. (2017) Glaucoma. Lancet 390, 2183-2193.
16. Križaj D. (2019) What is glaucoma? In: Kolb H, Fernandez E, Nelson R, editors. The Organization of the Retina and Visual System. Salt Lake City (UT): University of Utah Health Sciences Center.

17. Choquet, H., Paylakhi, S., Kneeland, S.C., Thai, K.K., Hoffmann, T.J., Yin, J., Kvale, M.N., Banda, Y., Tolman, N.G., Williams, P.A., Schaefer, C., Melles, R.B., Risch, N., John, S.W.M., Nair, K.S., Jorgenson, E. (2018) A multiethnic genome-wide association study of primary open-angle glaucoma identifies novel risk loci. Nat Commun 9, 2278.
18. Iglesias, A.I., Springelkamp, H., Ramdas, W.D., Klaver, C.C., Willemsen, R., van Duijn, C.M. (2015) Genes, pathways, and animal models in primary open-angle glaucoma. Eye 29, 1285-1298.
19. Rao, P.V., Pattabiraman, P.P., Kopczynski, C. (2017) Role of the Rho GTPase/Rho kinase signaling pathway in pathogenesis and treatment of glaucoma: Bench to bedside research. *Exp Eye Res.* 158, 23-32.
20. Yarishkin, O., Baumann, J.M., Križaj, D. (2019) Mechano-electrical transduction in trabecular meshwork involves parallel activation of TRPV4 and TREK-1 channels. Channels 13, 168-171.
21. Yarishkin, O., Phuong, T.T.T., Baumann, J.M., de Ieso, M., Vazquez-Chona, F., Rudzitis, C.N., Sundberg, C., Lakk, M., Stamer, D.W., Križaj D**.** (2020) Mechanotransduction and dynamic outflow regulation in trabecular meshwork require Piezo1 channels. J Physiol, Nov 23
22. Aribindi, K., Guerra, Y., Lee, R.K., Bhattacharya, S.K. (2013) Comparative phospholipid profiles of control and glaucomatous human trabecular meshwork. Invest Ophthalmol Vis Sci. 54, 3037-3044.
23. Vahabikashi, A., Gelman, A., Dong, B., Gong, L., Cha, E.D.K., Schimmel, M., Tamm, E.R., Perkumas, K., Stamer, W.D., Sun, C., Zhang, H.F., Gong, H., Johnson, M. (2019) Increased stiffness and flow resistance of the inner wall of Schlemm's canal in glaucomatous human eyes. *Proc Natl Acad Sci U S A.* 116, 26555 - 26563

24. Ryskamp, D.A., Frye, A.M., Phuong, T.T., Yarishkin, O., Jo, A.O., Xu, Y., Lakk, M., Iuso, A., Redmon, S.N., Ambati, B., Hageman, G., Prestwich, G.D., Torrejon, K.Y., Križaj, D. (2016) TRPV4 regulates calcium homeostasis, cytoskeletal remodeling, conventional outflow and intraocular pressure in the mammalian eye. Sci Rep. 6:30583.
25. Lakk, M., Križaj D. (2020) Mechanoreciprocity requires interactions between TRPV4 channels, the Rho pathway and actin cytoskeleton. *bioRxiv* https://doi.org/10.1101/2020.08.11.24717
26. Rocio Servin-Vences, M.R., Moroni, M., Lewin, G.R., Poole, K. (2017) Direct measurement of TRPV4 and PIEZO1 activity reveals multiple mechanotransduction pathways in chondrocytes. *Elife*. 6, e21074.
27. Iuso, A., Križaj, D. (2016) TRPV4-AQP4 interactions 'turbocharge' astroglial sensitivity to small osmotic gradients. Channels 10, 172-174.
28. Kumari, S., Kumar, A., Sardar, P., Yadav, M., Majhi, R.K., Kumar, A., Goswami, C. (2015) Influence of membrane cholesterol in the molecular evolution and functional regulation of TRPV4. Biochem Biophys Res Commun 456, 312-319.
29. Saliez, J., Bouzin, C., Rath, G., Ghisdal, P., Desjardins, F., Rezzani, R., Rodella, L.F., Vriens, J., Nilius, B., Feron, O., Balligand, J.L., Dessy, C. (2008) Role of caveolar compartmentation in endothelium-derived hyperpolarizing factor-mediated relaxation: Ca2+ signals and gap junction function are regulated by caveolin in endothelial cells. Circulation 117, 1065-1074.
30. Gimpl, G., Gehrig-Burger, K. (2011) Probes for studying cholesterol binding and cell biology. Steroids. 76, 216-231.

31. Wei, H., Malcor, J.M., Harper, M.T. (2018) Lipid rafts are essential for release of phosphatidylserine-exposing extracellular vesicles from platelets. Sci Rep. 8, 9987.

32. Zidovetzki, R., Levitan, I. (2007) Use of cyclodextrins to manipulate plasma membrane cholesterol content: evidence, misconceptions and control strategies. Biochim Biophys Acta. 1768, 1311- 1324.

33. Christian, A. E., Haynes, M. P., Phillips, M. C., Rothblat, G. H. (1997) Use of cyclodextrins for manipulating cellular cholesterol content. J. Lipid Res 38, 2264–2272.

34. Pattabiraman, P.P., Rinkoski, T., Poeschla, E., Proia, A., Challa, .P, Rao, P.V. (2015) RhoA GTPase-induced ocular hypertension in a rodent model is associated with increased fibrogenic activity in the trabecular meshwork. Am J Pathol 185, 496-512.

35. Tumminia, S.J., Mitton, K.P., Arora, J., Zelenka, P., Epstein, D.L., Russell, P. (1998) Mechanical stretch alters the actin cytoskeletal network and signal transduction in human trabecular meshwork cells. Invest Ophthalmol Vis Sci. 39, 1361-1371.

36. Strotmann, R., Harteneck, C., Nunnenmacher, K., Schultz, G., Plant, T.D. (2000) OTRPC4, a nonselective cation channel that confers sensitivity to extracellular osmolarity. Nat Cell Biol. 2, 695-702.

37. Liedtke, W., Choe, Y., Martí-Renom, M.A, Bell, A.M., Denis, C.S., Sali, A., Hudspeth, A.J., Friedman, J.M., Heller, S. V(2000) Vanilloid receptor-related osmotically activated channel (VR-OAC), a candidate vertebrate osmoreceptor. Cell 103, 525-535.

38. Toft-Bertelsen, T.L., Križaj, D., MacAulay, N. (2017) When size matters: transient receptor potential vanilloid 4 channel as a volume-sensor rather than an osmo-sensor. J Physiol. 595, 3287-3302.

39. Jo, A.O., Lakk, M., Frye, A.M., Phuong, T.T.T., Redmon, S.N., Roberts, R., Berkowitz, B.A., Yarishkin, O., Križaj, D. (2016) Differential volume regulation and calcium signaling in two ciliary body cell types is subserved by TRPV4 channels. Proc Natl Acad Sci U S A. 113, 3885-3890.
40. Jo, A.O., Ryskamp, D.A., Phuong, T.T.T., Verkman, A.S., Yarishkin, O., MacAulay, N., Križaj, D. (2015) TRPV4 and AQP4 Channels Synergistically Regulate Cell Volume and Calcium Homeostasis in Retinal Müller Glia. J Neurosci 35, 13525-13537.
41. Phuong, T.T.T., Redmon, S.N., Yarishkin, O., Winter, J.M., Li, D.Y., Križaj, D. (2017) Calcium influx through TRPV4 channels modulates the adherens contacts between retinal microvascular endothelial cells. J Physiol. 595, 6869-6885.
42. Lapajne, L., Lakk, M., Yarishkin, O., Gubeljak, L., Hawlina, M., Križaj, D. (2020) Polymodal Sensory Transduction in Mouse Corneal Epithelial Cells. Invest Ophthalmol Vis Sci. 61, 2.
43. White, J.P., Cibelli, M., Urban, L., Nilius, B., McGeown, J.G., Nagy, I. (2016) TRPV4: Molecular Conductor of a Diverse Orchestra. *Physiol Rev*. 96, 911-973.
44. Toft-Bertelsen, T.L., Yarishkin, O., Redmon, S., Phuong, T.T.T., Križaj, D., MacAulay, N. (2019) Volume sensing in the transient receptor potential vanilloid 4 ion channel is cell type-specific and mediated by an N-terminal volume-sensing domain. J Biol Chem 294, 18421-18434.
45. Grierson, I., Lee, W.R. (1975) Pressure-induced changes in the ultrastructure of the endothelium lining Schlemm's canal. Am J Ophthalmol 80, 863-884.

46. Johnstone, M.A. (2004) The aqueous outflow system as a mechanical pump: evidence from examination of tissue and aqueous movement in human and non-human primates. J Glaucoma. 13, 421-438.

47. Sherwood, J.M., Stamer, W.D., Overby, D.R. (2019) A model of the oscillatory mechanical forces in the conventional outflow pathway. J R Soc Interface. 16, 20180652.

48. Morenilla-Palao, C., Pertusa, M., Meseguer, V., Cabedo, H., Viana, F. (2009) Lipid raft segregation modulates TRPM8 channel activity. J Biol Chem 284, 9215-9224.

49. Naylor, J., Li, J., Milligan, C.J., Zeng, F., Sukumar, P., Hou, B., Sedom A., Yuldasheva, N., Majeed, Y., Beri, D., Jiang, S., Seymour, V.A., McKeown, L., Kumar, B., Harteneck, C., O'Regan, D., Wheatcroft, S.B., Kearney, M.T., Jones, C., Porter, K.E., Beech, D.J. (2010) Pregnenolone sulphate- and cholesterol-regulated TRPM3 channels coupled to vascular smooth muscle secretion and contraction. Circ Res 106, 1507-1515.

50. Picazo-Juárez, G. , Romero-Suárez, S., Nieto-Posadas, A., Llorente I, Jara-Oseguera, A., Briggs, M., McIntosh, T.J., Simon, S.A., Ladrón-de-Guevara, E., Islas, L.D., Rosenbaum, T. (2011) Identification of a binding motif in the S5 helix that confers cholesterol sensitivity to the TRPV1 ion channel. J Biol Chem 286, 24966-24976.

51. Berna-Erro, A., Izquierdo-Serra, M., Sepúlveda, R.V., Rubio-Moscardo, F., Doñate-Macián, P., Serra, S.A., Carrillo-Garcia, J., Perálvarez-Marín, A., González-Nilo, F., Fernández-Fernández, J.M., Valverde, M.A. (2017) Structural determinants of 5',6'-epoxyeicosatrienoic acid binding to and activation of TRPV4 channel. Sci Rep 7, 10522.

52. Redmon, S.N., Shibasaki, K., Križaj, D. (2017) Transient receptor potential cation channel subfamily V member 4 (TRPV4). Encyclopedia of Signaling Molecules. Ed. Choi, S., Springer Nature, New York.

53. Santiago, J., Guzmàn, G.R., Rojas, L.V., Marti, R., Asmar-Rovira, G.A., Santana, L.F., McNamee, M., Lasalde-Dominicci, J.A. (2001) Probing the effects of membrane cholesterol in the Torpedo californica acetylcholine receptor and the novel lipid-exposed mutation alpha C418W in Xenopus oocytes. J Biol Chem 276, 46523-46532.

54. Bratengeier, C., Liszka, A., Hoffman, J., Bakker, A.D., Fahlgren, A. (2020) High shear stress amplitude in combination with prolonged stimulus duration determine induction of osteoclast formation by hematopoietic progenitor cells. FASEB J 34, 3755-3772.

55. Gavara, N., Chadwick, RS. (2016) Relationship between cell stiffness and stress fiber amount, assessed by simultaneous atomic force microscopy and live-cell fluorescence imaging. Biomech Model Mechanobiol 15, 511-523.

56. Graziani, A., Bricko, V., Carmignani, M., Graier, W.F., Groschner, K. (2004) Cholesterol- and caveolin-rich membrane domains are essential for phospholipase A2-dependent EDHF formation. Cardiovasc Res 64, 234-242.

57. Levitan, I., Christian, A.E., Tulenko, T.N., Rothblat, G.H. (2000) Membrane cholesterol content modulates activation of volume-regulated anion current in bovine endothelial cells. J Gen Physiol 115, 405-416.

58. Byfield, F.J., Aranda-Espinoza, H., Romanenko, V.G., Rothblat, G.H., Levitan, I. (2004) Cholesterol depletion increases membrane stiffness of aortic endothelial cells. Biophys J 87, 3336-3343.

59. Kenworthy, A.K., Nichols, B.J., Remmert, C.L., Hendrix, G.M., Kumar, M., Zimmerberg, J., Lippincott-Schwartz, J. (2004) Dynamics of putative raft-associated proteins at the cell surface.J Cell Biol 165, 735-746.

60. Vrljic, M., Nishimura, S.Y., Moerner, W.E., McConnell, H.M. (2005) Cholesterol depletion suppresses the translational diffusion of class II major histocompatibility complex proteins in the plasma membrane. Biophys J 88, 334-347.

61. Ridone, P., Pandzic, E., Vassalli, M., Cox, C.D., Macmillan, A., Gottlieb, P.A., Martinac, B. (2020) Disruption of membrane cholesterol organization impairs the activity of PIEZO1 channel clusters. J Gen Physiol 152, :e201912515.

62. Lakk, M., Yarishkin, O., Baumann, J.M., Iuso, A., Križaj, D. (2017) Cholesterol regulates polymodal sensory transduction in Müller glia. Glia 65, 2038-2050.

63. Lei, L., Lu, S., Wang, Y., Kim, T., Mehta, D., Wang, Y. (2014) The role of mechanical tension on lipid raft dependent PDGF-induced TRPC6 activation. Biomaterials 35, 2868-2877.

64. Lockwich, T.P., Liu, X., Singh, B.B., Jadlowiec, J., Weiland, S., Ambudkar, I.S. (2000) Assembly of Trp1 in a signaling complex associated with caveolin-scaffolding lipid raft domains. J Biol Chem 275(16):11934-42.

65. Sághy, É., Szőke, É., Payrits, M., Helyes, Z., Börzsei, R., Erostyák, J., Jánosi, T.Z., Sétáló, G., Szolcsányi, J. (2015) Evidence for the role of lipid rafts and sphingomyelin in Ca2+-gating of Transient Receptor Potential channels in trigeminal sensory neurons and peripheral nerve terminals. Pharmacol Res 100, 101-116.

66. Peters, M., Katz, B., Lev, S., Zaguri, R., Gutorov, R., Minke, B. (2017) Depletion of Membrane Cholesterol Suppresses Drosophila Transient Receptor Potential-Like (TRPL) Channel Activity. Curr Top Membr 80, 233-254.

67. Perozo, E., Kloda, A., Cortes, D.M., Martinac, B. (2002) Physical principles underlying the transduction of bilayer deformation forces during mechanosensitive channel gating. Nat Struct Biol 9, 696-703.

68. Anishkin, A., Loukin, S.H., Teng, J., Kung, C. (2014) Feeling the hidden mechanical forces in lipid bilayer is an original sense. Proc Natl Acad Sci USA 111, 7898–7905.

69. Bukiya, A.N., Belani, J.D., Rychnovsky, S., Dopico, A.M. (2011) Specificity of cholesterol and analogs to modulate BK channels points to direct sterol-channel protein interactions. J Gen Physiol 137, 93-110.

70. Lee, A.G. (2019) Interfacial Binding Sites for Cholesterol on TRP Ion Channels. Biophys J 117, 2020-2033.

71. Loukin, S.H., Su, Z., Kung, C. (2009) Hypotonic shocks activate rat TRPV4 in yeast in the absence of polyunsaturated fatty acids. FEBS Lett 583, 754-758.

72. Liu, M., Huang, W., Wu, D., Priestley, J.V. (2006) TRPV1, but not P2X, requires cholesterol for its function and membrane expression in rat nociceptors. Eur J Neurosci 24, 1-6.

73. Szoke, E., Börzsei, R., Tóth, D.M., Lengl, O., Helyes, Z., Sándor, Z., Szolcsányi, J. (2010) Effect of lipid raft disruption on TRPV1 receptor activation of trigeminal sensory neurons and transfected cell line. Eur J Pharmacol 628, 67-74.

74. Startek, J.B., Boonen, B., López-Requena, A., Talavera, A., Alpizar, Y.A., Ghosh, D., Van Ranst, N., Nilius, B., Voets, T., Talavera, K. (2019) Mouse TRPA1 function and membrane localization are modulated by direct interactions with cholesterol. Elife 8:e46084.

75. Teng, J., Loukin, S.H., Anishkin, A., Kung, C. (2015) L596-W733 bond between the start of the S4-S5 linker and the TRP box stabilizes the closed state of TRPV4 channel. Proc Natl Acad Sci U S A 112, 3386-3391.

76. Klausen, T.K., Janssens, A., Prenen, J., Owsianik, G., Hoffmann, E.K., Pedersen, S.F., Nilius, B. (2014) Single point mutations of aromatic residues in transmembrane helices 5 and -6 differentially affect TRPV4 activation by 4α-PDD and hypotonicity: implications for the role of the pore region in regulating TRPV4 activity. Cell Calcium 55, 38-47.

77. Balse, E., El-Haou, S., Dillanian, G., Dauphin, A., Eldstrom, J., Fedida, F., Coulombe, A., Hatem, S.N. (2009) Cholesterol modulates the recruitment of Kv1.5 channels from Rab11-associated recycling endosome in native atrial myocytes. Proc Natl Acad Sci U S A 106, 14681-14686.

78. Romanenko VG, Fang Y, Byfield F, Travis AJ, Vandenberg CA, Rothblat GH, Levitan I. Cholesterol sensitivity and lipid raft targeting of Kir2.1 channels. Biophys J. 2004 Dec;87(6):3850-61.

79. Saha S, Ghosh A, Tiwari N, Kumar A, Kumar A, Goswami C. Preferential selection of Arginine at the lipid-water-interface of TRPV1 during vertebrate evolution correlates with its snorkeling behaviour and cholesterol interaction. Sci Rep. 2017 Dec 1;7(1):16808.

80. Klausen TK, Hougaard C, Hoffmann EK, Pedersen SF. Cholesterol modulates the volume-regulated anion current in Ehrlich-Lettre ascites cells via effects on Rho and F-actin. Am J Physiol Cell Physiol. 2006 Oct;291(4):C757-71.

81. Chubinskiy-Nadezhdin VI, Efremova TN, Khaitlina SY, Morachevskaya EA. Functional impact of cholesterol sequestration on actin cytoskeleton in normal and transformed fibroblasts. Cell Biol Int. 2013 Jun;37(6):617-23.

82. Hissa B, Oakes PW, Pontes B, Juan GR-S, Gardel ML. Cholesterol depletion impairs contractile machinery in neonatal rat cardiomyocytes. Scientific Reports. Springer Nature. 2017;7:43764.

83. Sun M, Northup N, Marga F, Huber T, Byfield FJ, Levitan I, et al. The effect of cellular cholesterol on membrane-cytoskeleton adhesion. Journal of Cell Science. 2007;120:2223-2231.

84. Okamoto T, Schlegel A, Scherer PE, Lisanti MP. Caveolins, a family of scaffolding proteins for organizing "preassembled signaling complexes" at the plasma membrane. J Biol Chem. 1998 Mar 6;273(10):5419-22.

85. Aga M, Bradley JM, Wanchu R, Yang Y, Acott TS, Keller KE. Differential effects of caveolin-1 and -2 knockdown on aqueous outflow and altered extracellular matrix turnover in caveolin-silenced trabecular meshwork cells. Invest Ophthalmol Vis Sci. 2014 Aug 7;55(9):5497-509.

86. Elliott MH, Ashpole NE, Gu X, Herrnberger L, McClellan ME, Griffith GL, Reagan AM, Boyce TM, Tanito M, Tamm ER, Stamer WD. Caveolin-1 modulates intraocular pressure: implications for caveolae mechanoprotection in glaucoma. Sci Rep. 2016 Nov 14;6:37127.

87. Gerald McGwin Jr, Sandre McNeal, Cynthia Owsley, Christopher Girkin, David Epstein, Paul P Lee. Statins and other cholesterol-lowering medications and the presence of glaucoma. Arch Ophthalmol. 2004 Jun;122(6):822-6.

88. Thorleifsson et al. Common variants near CAV1 and CAV2 are associated with primary open-angle glaucoma. Nat Genet 2010 Oct;42(10):906-9.

89. Wiggs JL, Kang JH, Yaspan BL, Mirel DB, Laurie C, Crenshaw A, Brodeur W, Gogarten S, Olson LM, Abdrabou W, DelBono E, Loomis S, Haines JL, Pasquale LR; GENEVA Consortium. Common variants near CAV1 and CAV2 are associated with primary open-angle glaucoma in Caucasians from the USA. Hum Mol Genet. 2011 Dec 1;20(23):4707-13.

90. Yarishkin O, Phuong TTT, Bretz CA, Olsen KW, Baumann JM, Lakk M, Crandall A, Heurteaux C, Hartnett ME, Križaj D. TREK-1 channels regulate pressure sensitivity and calcium signaling in trabecular meshwork cells. J Gen Physiol. 2018 Dec 3;150(12):1660-1675.

91. Grundy D. Principles and standards for reporting animal experiments in the journal of physiology and experimental physiology. J Physiol 2015 593, 2547–2549.

92. Krizaj, D., Gorusupudi, A., Bernstein, P., Toft-Bertelsen, T., Macaulay, N., Lakk, M., Krizaj, D. (2020) Cholesterol regulates TRPV4-dependent signaling in the trabecular meshwork. Invest Ophthalmol Vis Sci 61, 3424-3424.

93. Folch, J., Lees, M., Stanley, G.H. (1957) A simple method for the isolation and purification of total lipides from animal tissues. J Biol Chem 226, 497-509.

94. Lakk, M., Young, D., Baumann, J.M., Jo, A.O., Hu, H., Križaj, D. (2018) Polymodal TRPV1 and TRPV4 Sensors Colocalize but Do Not Functionally Interact in a Subpopulation of Mouse Retinal Ganglion Cells. Front Cell Neurosci 12, 353.

95. Ryskamp, D.A., Witkovsky, P., Barabas, P., Huang, W., Koehler, C., Akimov, N.P., Lee, S.H., Chauhan, S., Xing, W., Rentería, R.C., Liedtke, W., Krizaj, D. (2011) The

polymodal ion channel transient receptor potential vanilloid 4 modulates calcium flux, spiking rate, and apoptosis of mouse retinal ganglion cells. J Neurosci 31, 7089-7101.

96. Ryskamp, D.A., Jo, A.O., Frye, A.M., Vazquez-Chona, F., MacAulay, N., Thoreson, W.B., Križaj, D. (2014) Swelling and eicosanoid metabolites differentially gate TRPV4 channels in retinal neurons and glia. J Neurosci 34, 15689-156700.
97. Molnar, T., Barabas, P., Birnbaumer, L., Punzo, C., Kefalov, V., Križaj, D. (2012) Store-operated channels regulate intracellular calcium in mammalian rods. J Physiol 590, 3465-3481.
98. Fenton, R.A., Moeller, H.B., Zelenina, M., Snaebjornsson, M.T., Holen, T., MacAulay, N. (2010) Differential water permeability and regulation of three aquaporin 4 isoforms. Cell Mol Life Sci 67, 829-840.
99. Hamann, S., Herrera-Perez, J.J., Zeuthen, T., Alvarez-Leefmans, F.J. (2010) Cotransport of water by the Na+-K+-2Cl(-) cotransporter NKCC1 in mammalian epithelial cells. J Physiol 588, 4089-4101.

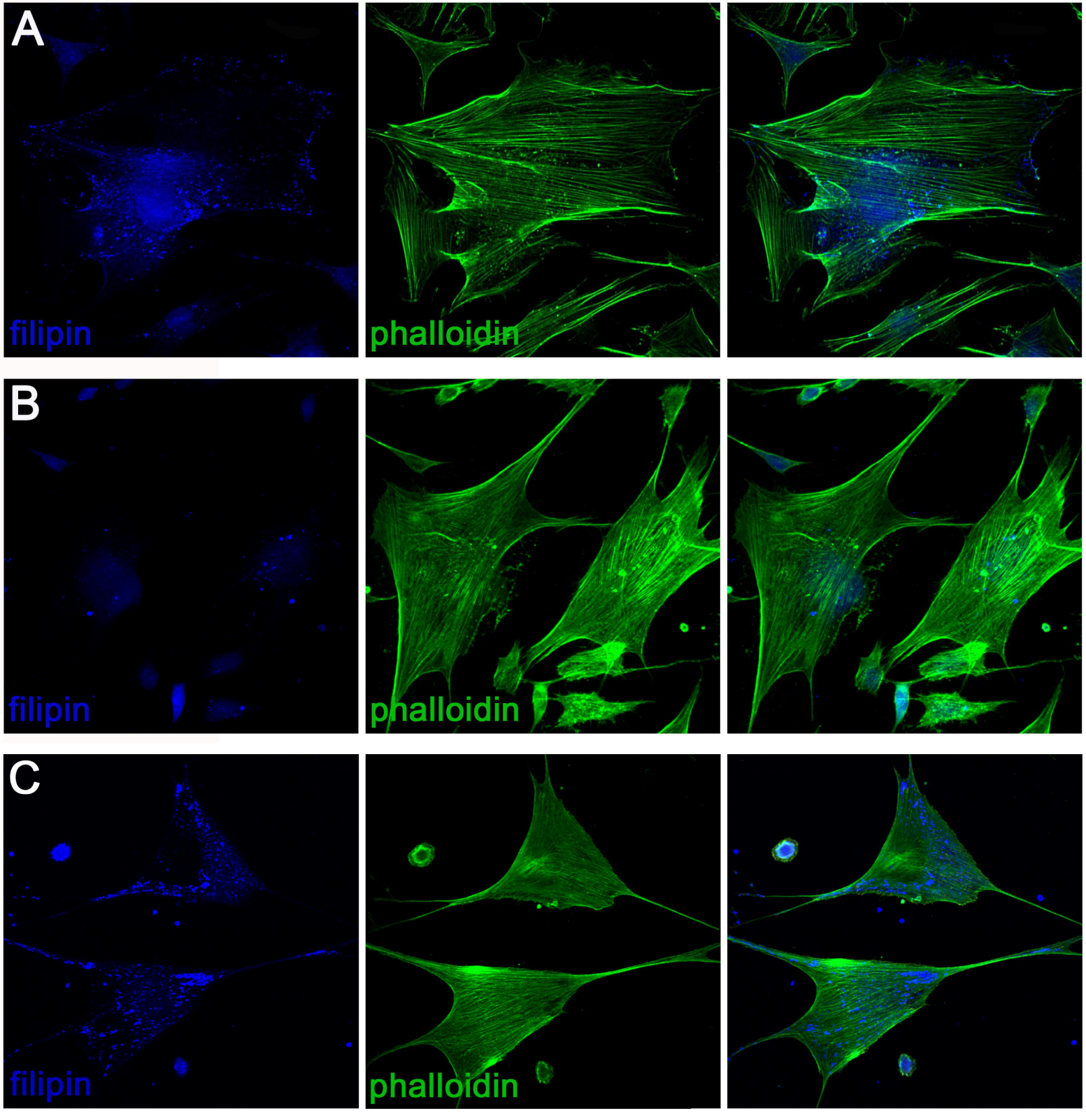
A
filipin
phalloidin
B
filipin
phalloidin
C
filipin
phalloidin

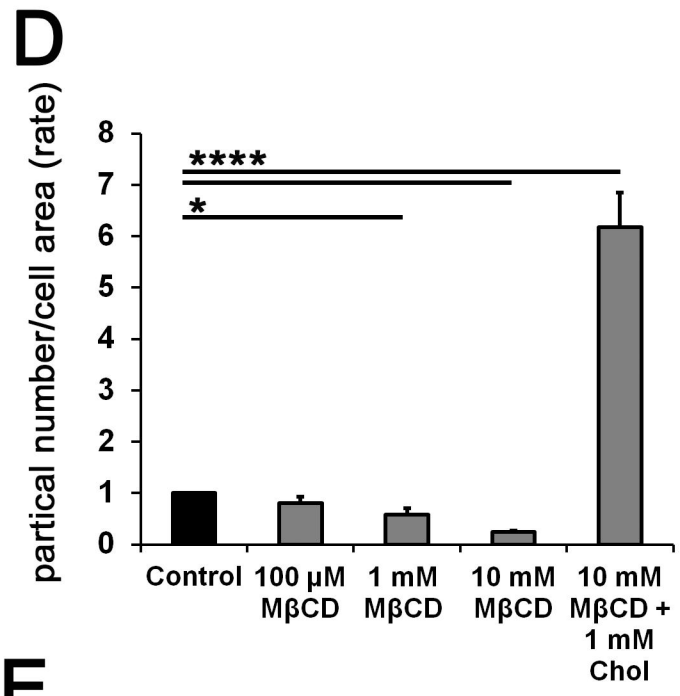
D
partical number/cell area (rate)
0
1
2
3
4
5
6
7
8
****
*
Control
100 μM MβCD
1 mM MβCD
10 mM MβCD
10 mM MβCD + 1 mM Chol

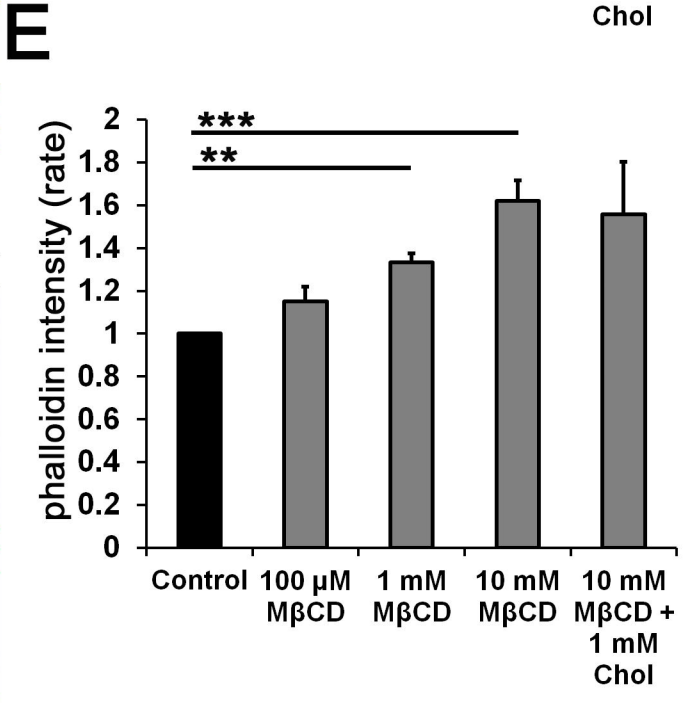
E
phalloidin intensity (rate)
0
0.2
0.4
0.6
0.8
1
1.2
1.4
1.6
1.8
2
***
**
Control
100 μM MβCD
1 mM MβCD
10 mM MβCD
10 mM MβCD + 1 mM Chol

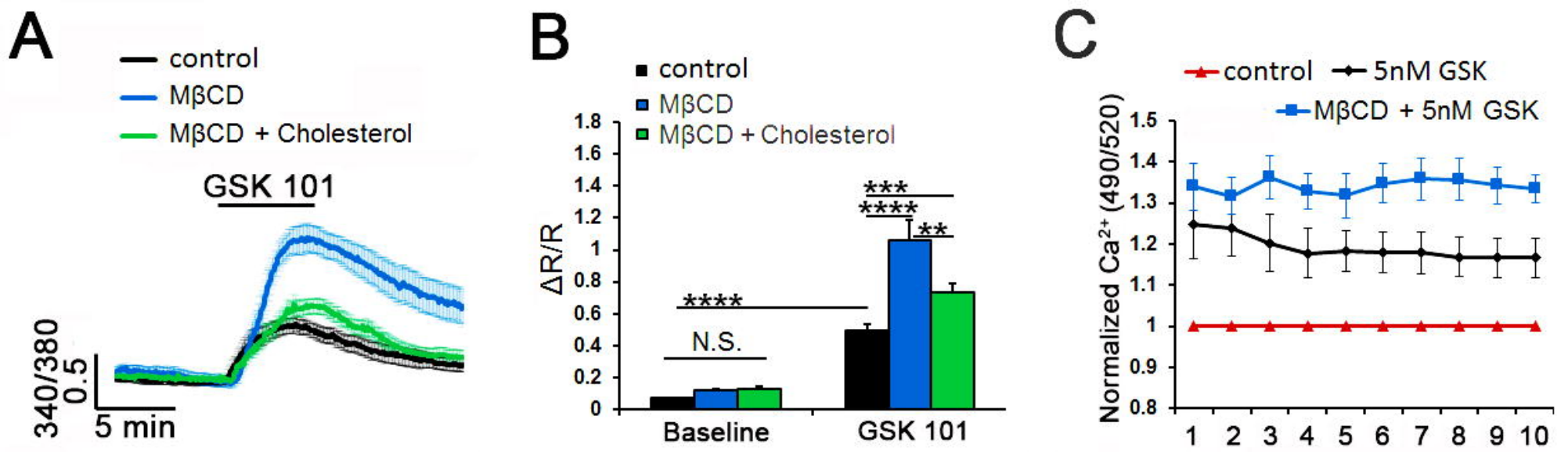
A
control
MβCD
MβCD + Cholesterol
GSK 101
340/380
0.5
5 min
B
control
MβCD
MβCD + Cholesterol
ΔR/R
1.8
1.6
1.4
1.2
1
0.8
0.6
0.4
0.2
0
****
N.S.
***
****
**
Baseline
GSK 101
C
control
5nM GSK
MβCD + 5nM GSK
Normalized Ca2+ (490/520)
1.5
1.4
1.3
1.2
1.1
1
0.9
0.8
1
2
3
4
5
6
7
8
9
10

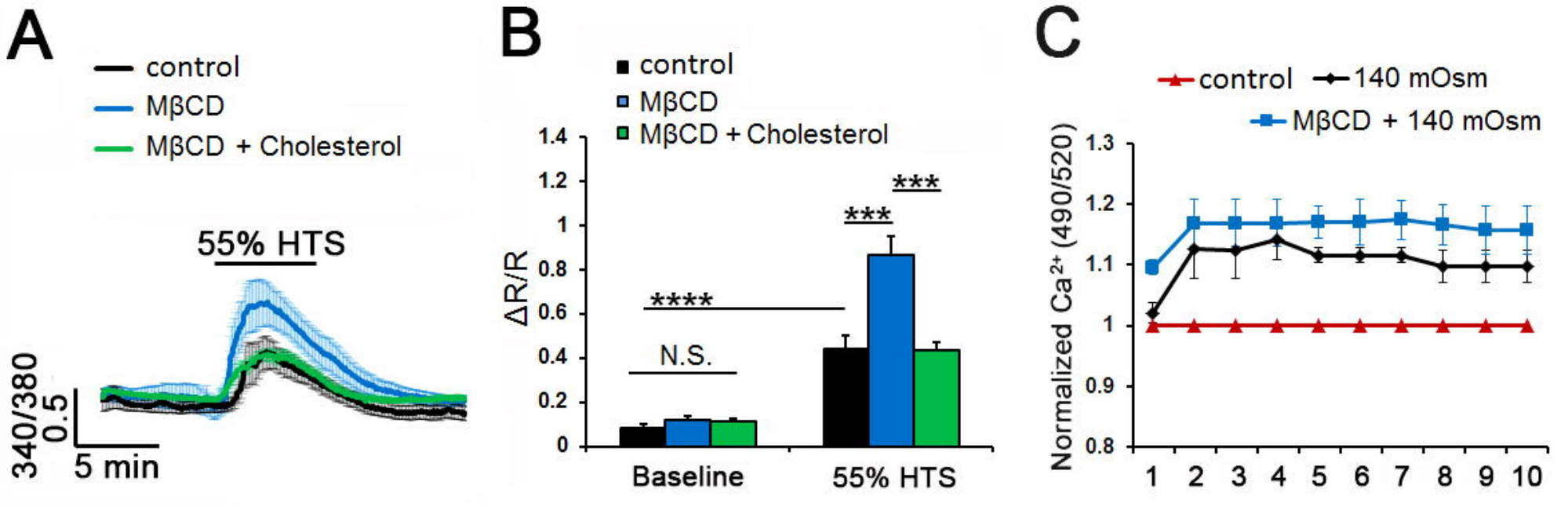
A
control
MβCD
MβCD + Cholesterol
55% HTS
340/380
0.5
5 min
B
control
MβCD
MβCD + Cholesterol
ΔR/R
1.4
1.2
1
0.8
0.6
0.4
0.2
0
****
N.S.
***
***
Baseline
55% HTS
C
control
140 mOsm
MβCD + 140 mOsm
Normalized Ca2+ (490/520)
1.3
1.2
1.1
1
0.9
0.8
1
2
3
4
5
6
7
8
9
10

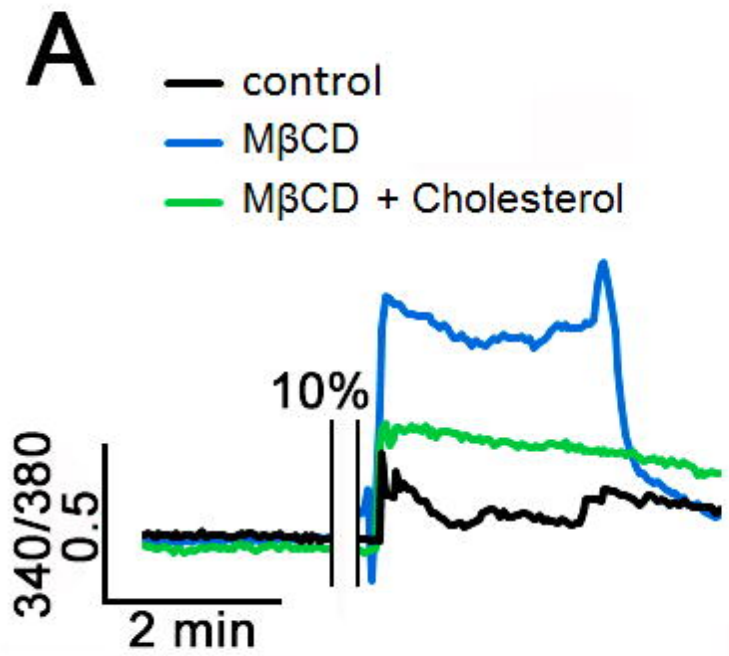
A
control
MβCD
MβCD + Cholesterol
10%
340/380
0.5
2 min

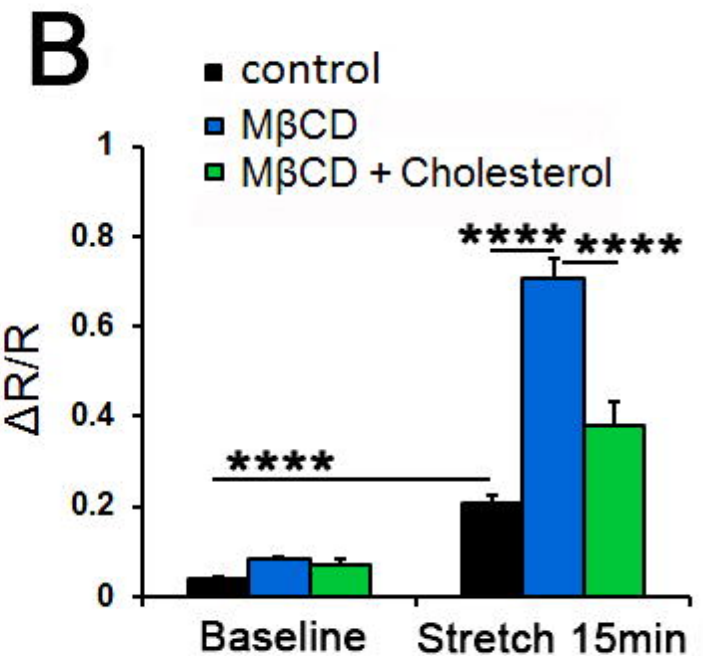
B
control
MβCD
MβCD + Cholesterol
ΔR/R
1
0.8
0.6
0.4
0.2
0
****
****
****
Baseline
Stretch 15min

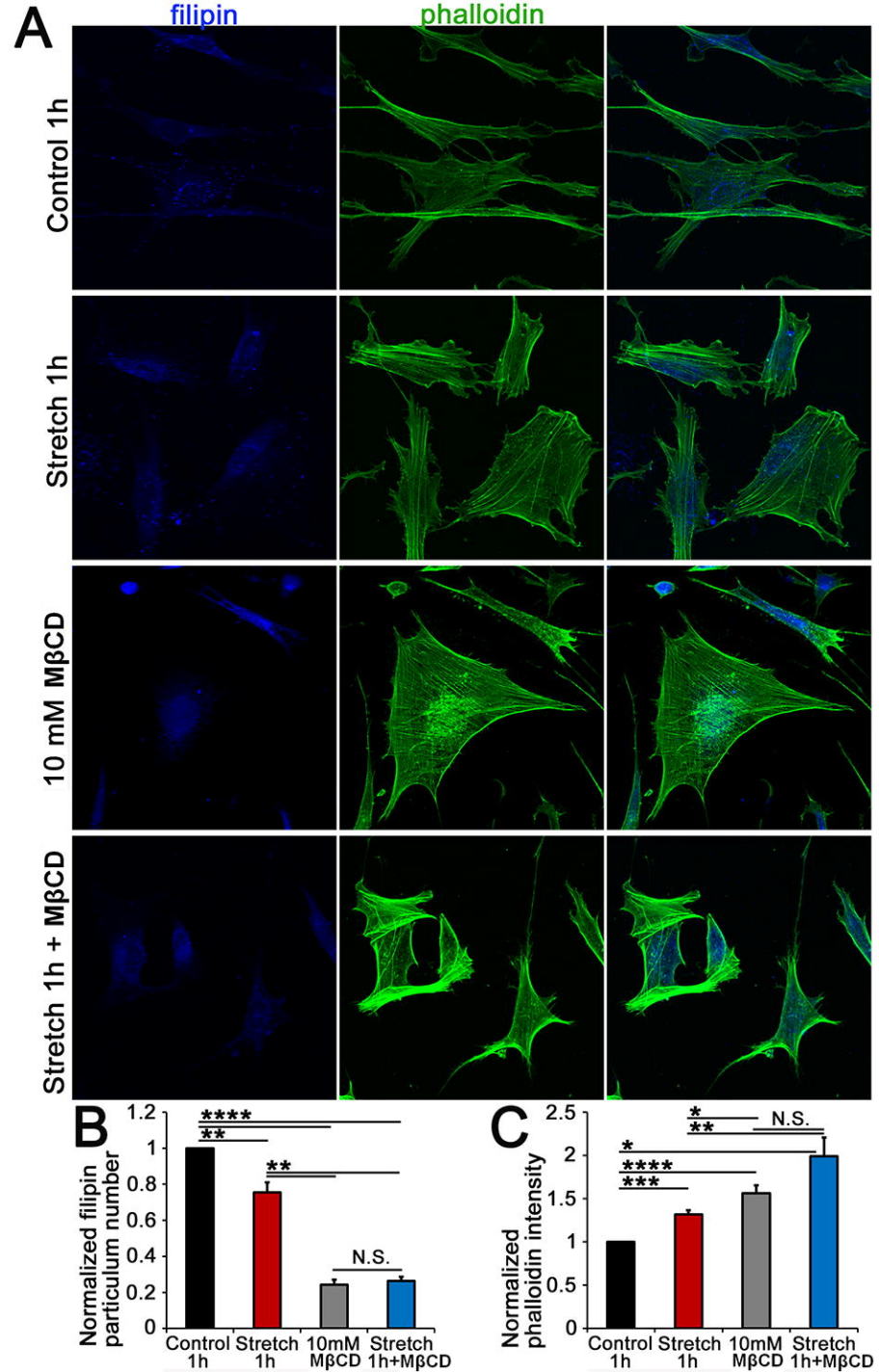
A
filipin
phalloidin
Control 1h
Stretch 1h
10 mM MβCD
Stretch 1h + MβCD
B
Normalized filipin particulum number
1.2
1
0.8
0.6
0.4
0.2
0
****
**
**
N.S.
Control 1h
Stretch 1h
10mM MβCD
Stretch 1h+MβCD
C
Normalized phalloidin intensity
2.5
2
1.5
1
0.5
0
*
**
N.S.
*
****
***
Control 1h
Stretch 1h
10mM MβCD
Stretch 1h+MβCD

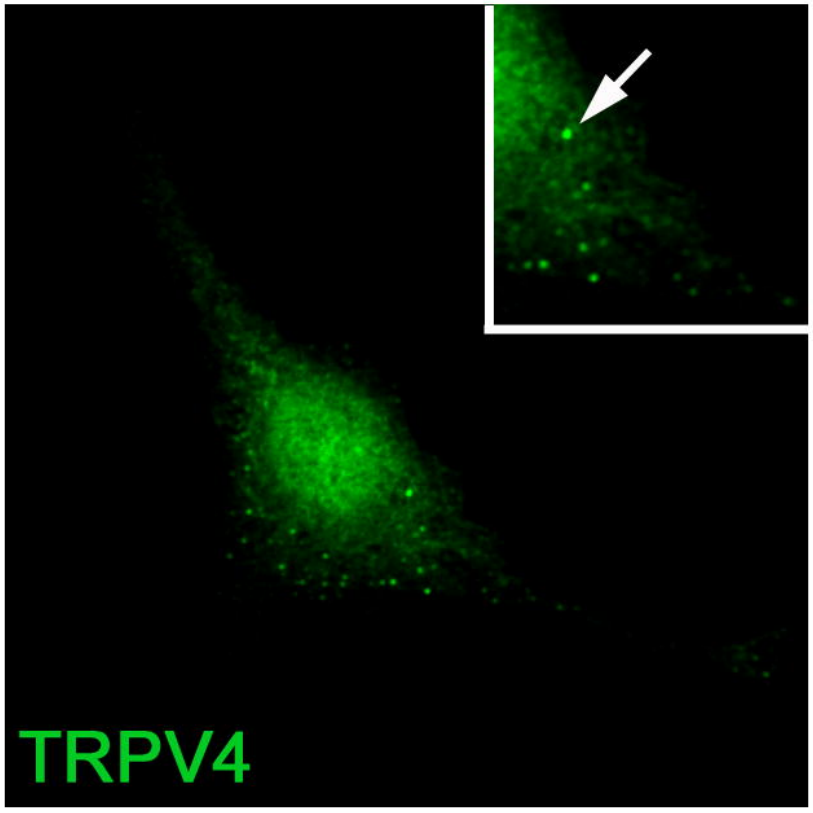
Control 1h
TRPV4

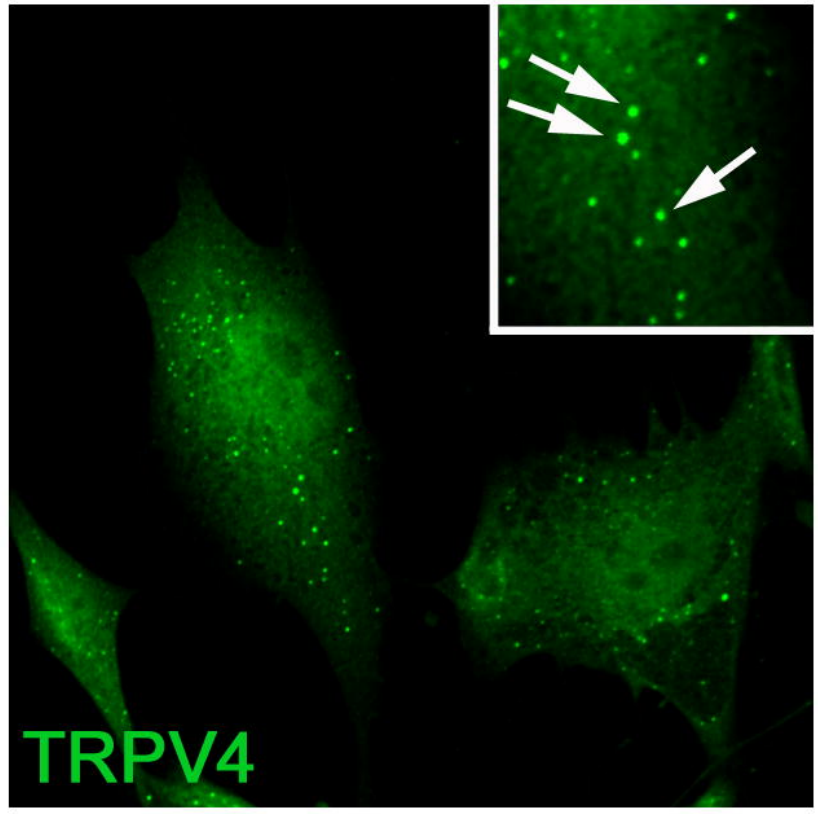
MβCD 1h
TRPV4

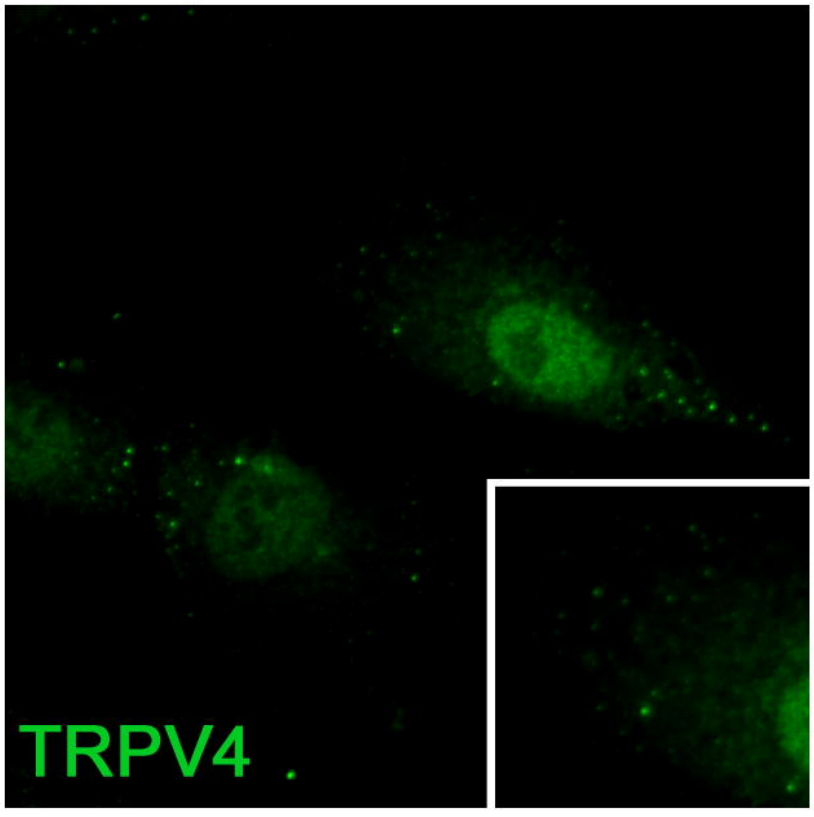
MβCD + Chol 1h
TRPV4

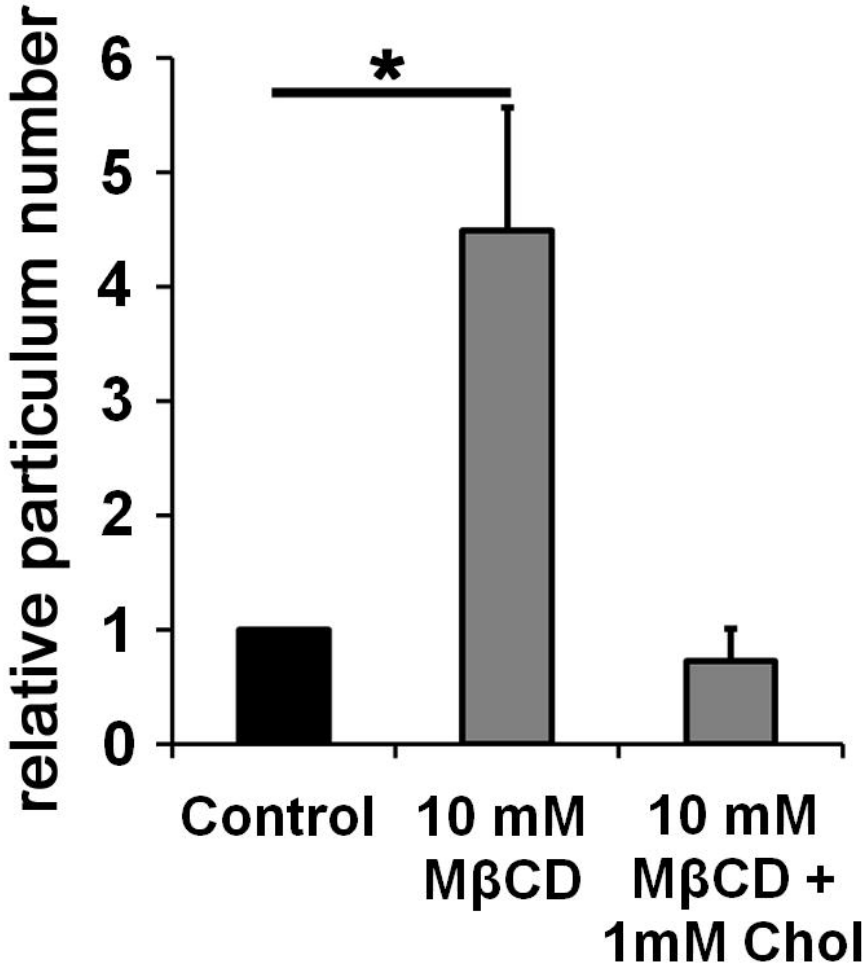
relative particulum number
0
1
2
3
4
5
6
*
Control
10 mM MβCD
10 mM MβCD + 1mM Chol

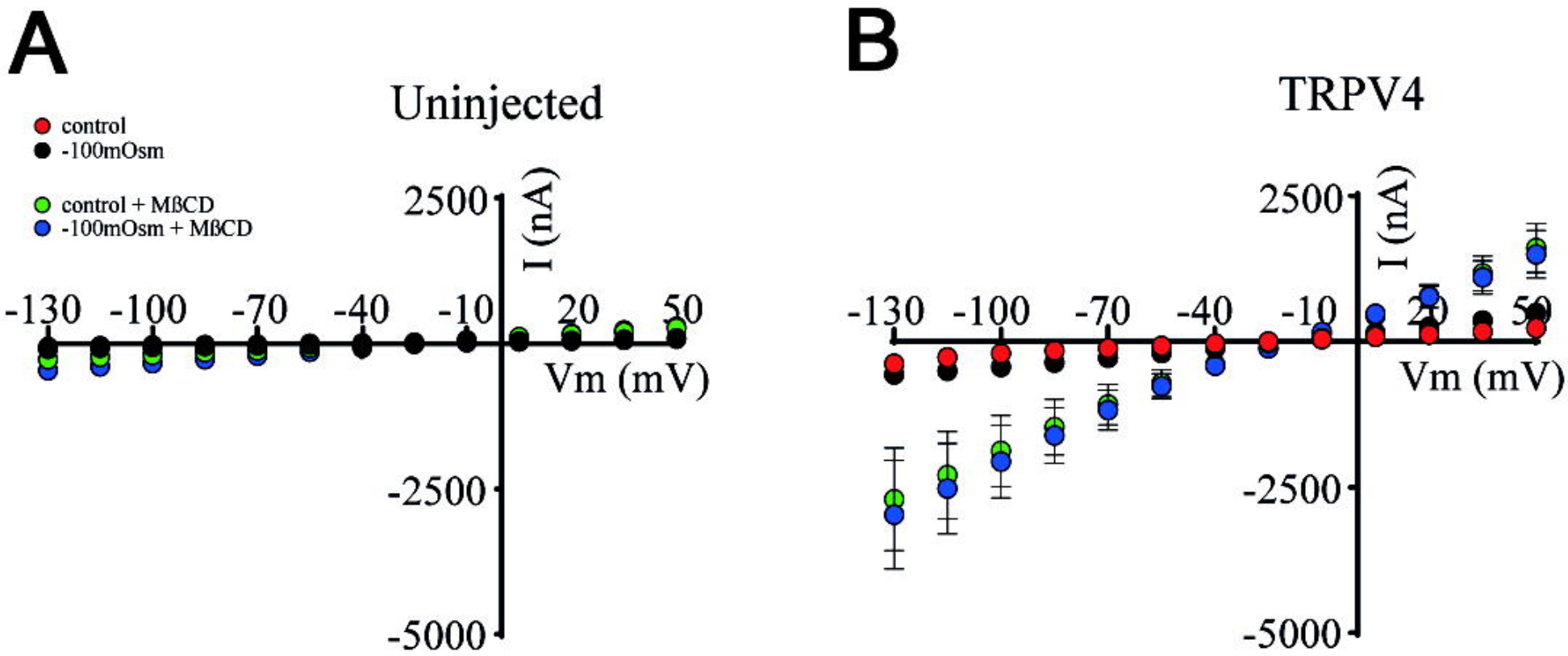
A
Uninjected
control
-100mOsm
control + MßCD
-100mOsm + MßCD
2500
I (nA)
-130
-100
-70
-40
-10
20
50
Vm (mV)
-2500
-5000
B
TRPV4
2500
I (nA)
-130
-100
-70
-40
-10
20
50
Vm (mV)
-2500
-5000

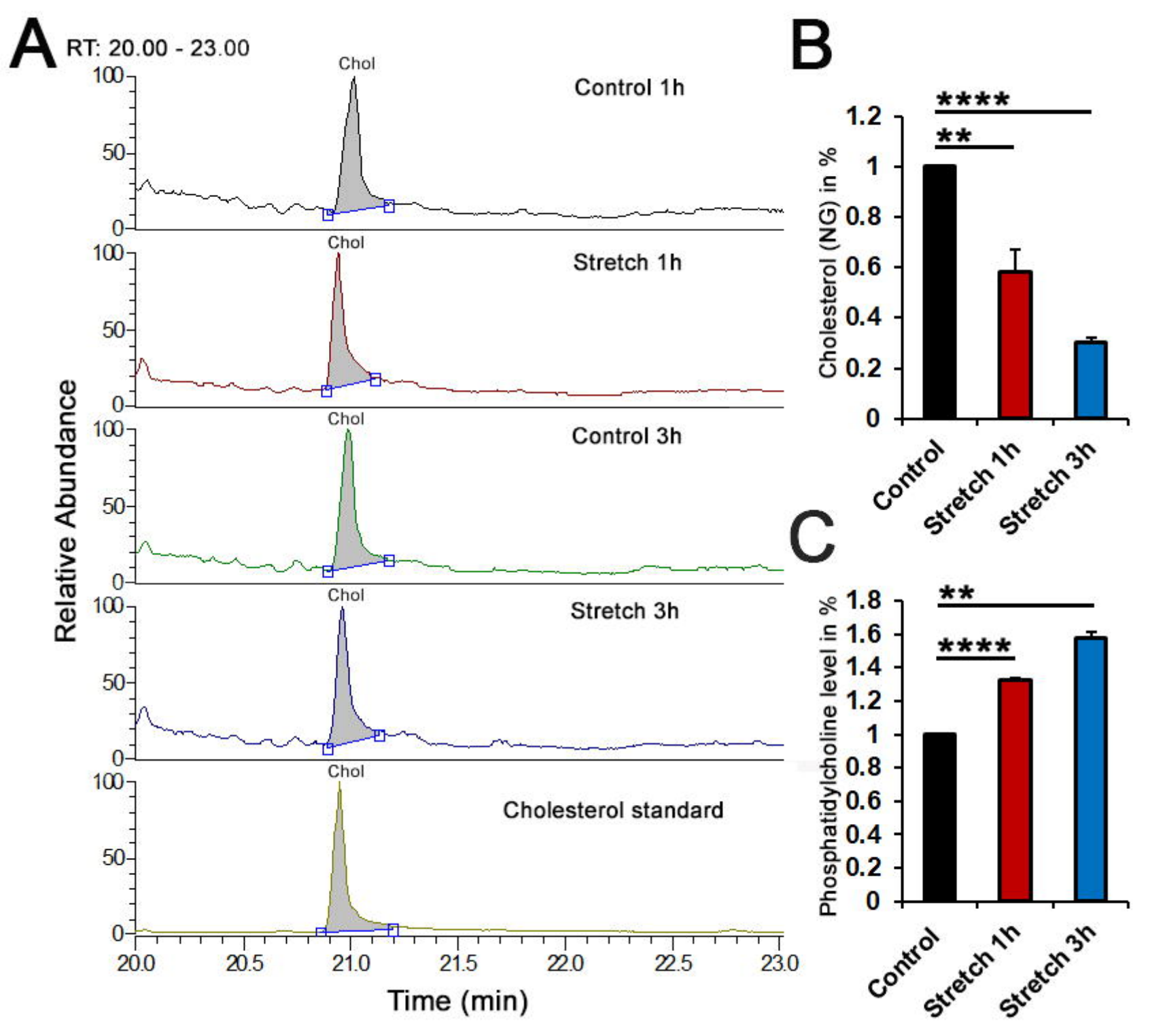
A
RT: 20.00 - 23.00
Chol
Control 1h
Stretch 1h
Control 3h
Stretch 3h
Cholesterol standard
Relative Abundance
Time (min)
B
Cholesterol (NG) in %
Control
Stretch 1h
Stretch 3h
C
Phosphatidylcholine level in %
Control
Stretch 1h
Stretch 3h